Transtensional deformation in the central Himalaya and its role in accommodating growth of the Himalayan orogen

Michael A. Murphy and Peter Copeland

Department of Geosciences, University of Houston, Houston, Texas, USA

Received 3 April 2004; revised 1 April 2005; accepted 19 April 2005; published 17 August 2005.

[1] Field mapping, structural analysis, and geochronologic data from northwestern Nepal reveal major normal right-slip motion along a previously unrecognized west-northwest striking system of shear zones that we term the Gurla Mandhata–Humla fault system (GMH). The GMH obliquely cuts across the Greater Himalayan Crystalline sequence and into the Lesser Himalayan imbricate thrust belt via two right-step-over structures. The average slip direction on the GMH parallels the strike of the Himalayan orogen. Motion along this fault system has resulted in an apparent left separation of the South Tibet Detachment, Main Central thrust zone, and Lesser Himalayan imbricate thrust belt along a north striking segment of the fault system. We estimate a minimum of 21 km of net slip on the southern branch of the GMH by restoring the trace of the Main Central thrust zone parallel to the average slip direction on the fault. Taking into account slip estimates from the northern branch of the GMH yields a minimum net slip estimate of 24.4 to 32.4 km for the GMH. The $^{232}Th/^{208}Pb$ ion microprobe monazite ages from leucogranite bodies indicate that motion on the GMH occurred after 15 Ma. Its initiation immediately followed crustal thickening between the Main Central thrust zone and Indus-Yalu suture zone. Motion on the GMH is contemporaneous with arc-normal contraction in the southernmost Himalayan orogen. These observations can be explained by a model that involves foreland propagating structural systems facilitating arc-normal contraction in the foreland and arc-parallel extension in the hinterland that work together to maintain the arcuate shape of the Himalayan orogen. **Citation:** Murphy, M. A., and P. Copeland (2005), Transtensional deformation in the central Himalaya and its role in accommodating growth of the Himalayan orogen, *Tectonics*, *24*, TC4012, doi:10.1029/2004TC001659.

1. Introduction

[2] Computation of strain partitioning between shortening and lateral extrusion during the Indo-Asian collision hinges on understanding the geometry, kinematics, slip rate, and life span of major crustal-scale faults. Although it is clear that the Himalaya absorbs a significant portion of the northward indentation of India through north-south shortening, the role of strike-slip and normal faulting in accommodating the convergence between India and Asia within the Tibetan Plateau remains debated. Two contrasting views dominate the debate: (1) deformation is localized along a few lithospheric-scale strike-slip faults separating rigid blocks resulting in lateral extrusion [e.g., *Tapponnier et al.*, 1982; *Peltzer and Tapponnier*, 1988; *Armijo et al.*, 1989; *Avouac and Tapponnier*, 1993; *Replumaz and Tapponnier*, 2003] and (2) deformation is distributed resulting in coeval east-west extension and north-south shortening within the interior of Tibet [e.g., *Rothery and Drury*, 1984; *Taylor et al.*, 2003; *Wright et al.*, 2004]. The lateral extrusion hypothesis requires large displacements on strike-slip faults that extend across the entire length of the extruded block. In contrast, the view that deformation is distributed considers internal deformation of the Tibetan Plateau to be accommodated by a greater number of faults with smaller displacements and correspondingly low slip rates.

[3] At the forefront of the debate over localized versus distributed deformation of Tibet is the role of the right-slip Karakoram fault. The fault lies along the southwest margin of the Tibet plateau and extends at least 800 km from the Pamirs in the north to the Mount Kailas area in the south (Figure 1). Slip estimates on the Karakoram fault vary widely from 120 km [e.g., *Searle*, 1996] to ~1000 km [*Peltzer and Tapponnier*, 1988]. Although large slip estimates (>600 km) imply the Karakoram fault has facilitated a large fraction of the convergence between India and Asia, lateral extrusion models also require the Karakoram fault to extend eastward from the Mount Kailas area along the suture between India and Asia for ~1000 km.

[4] Hypotheses for the large-scale geometry and evolution of the Karakoram fault fall into two general categories. *Peltzer and Tapponnier* [1988] suggest the fault transferred ~1000 km of right to the Indus-Yalu suture zone in the vicinity of the Mount Kailas area (Figure 2). More recently, *Lacassin et al.* [2004] interpret the Karakoram fault to have accumulated 600 km of right slip since 23 Ma and possibly as long as the past 34 Myr based on U-Pb ages of synkinematic igneous dikes within the shear zone. *Lacassin et al.* [2004] agree with the interpretation that the Karakoram fault transfers slip into the Indus-Yalu suture zone and further suggest the suture zone has accommodated significant tranpressional deformation. Alternatively, *Pêcher* [1991] suggested the Karakoram fault transfers slip

0278-7407/05/2004TC001659$12.00

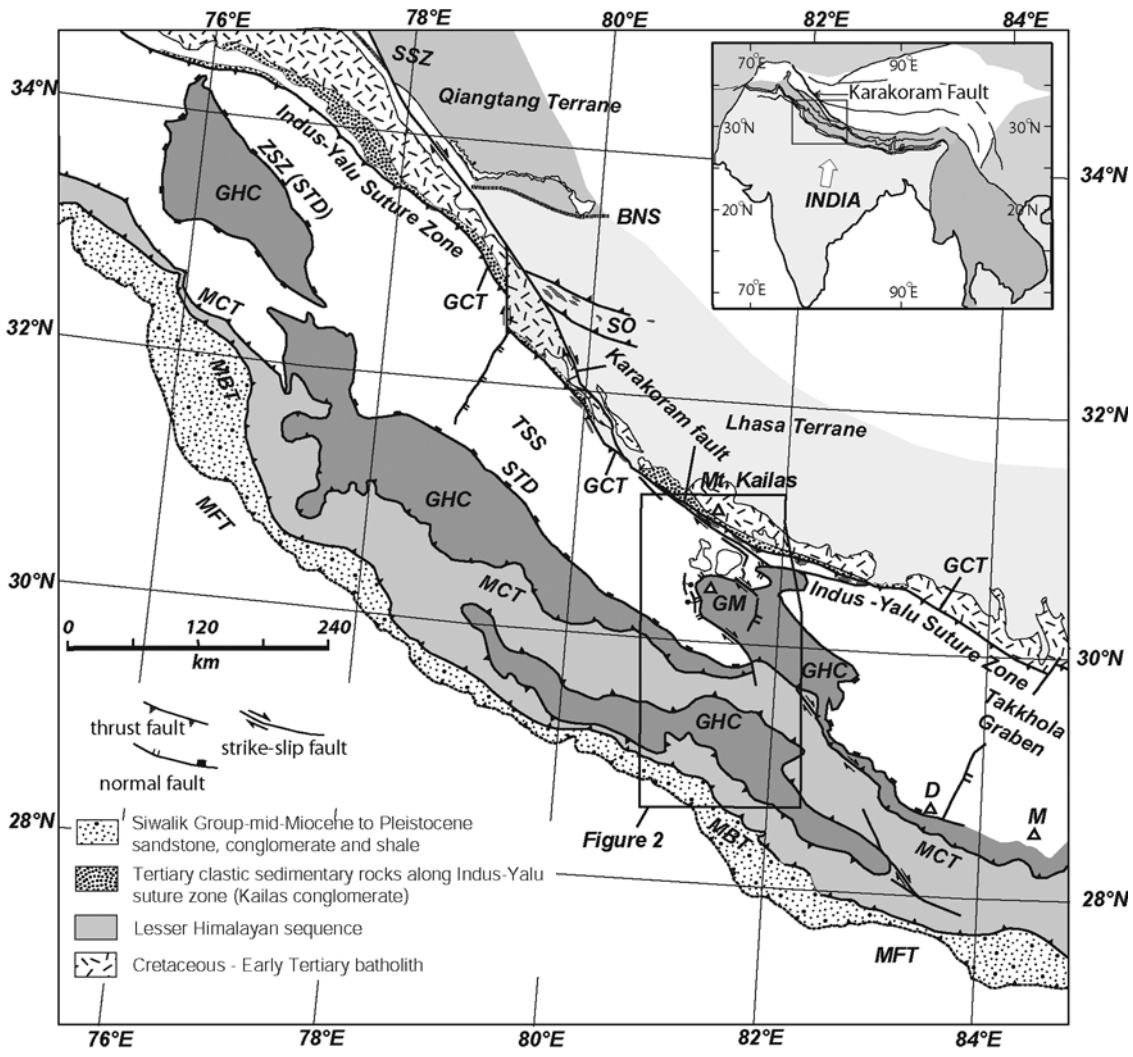

Figure 1. Tectonic map of the western Himalaya-Tibet orogen compiled from our field observations and previously published maps by *Cheng and Xu* [1987], *Searle* [1996], *Murphy et al.* [2000], *Murphy et al.* [2002], and *Yin* [2005]. Abbreviations are BNS, Banggong-Nuijiang suture zone; D, Daulaghiri; M, Manaslu; GCT, Great Counter thrust; GHC, Great Himalayan Complex; GM, Gurla Mandhata; MCT, Main Central thrust zone; MBT, Main Boundary thrust; MFT, Main Frontal thrust; SO, Shiquanhe ophiolite; SSZ, Shyok suture zone; STD, South Tibet Detachment; TSS, Tethyan Sedimentary Sequence; ZSZ, Zanskar shear zone.

to the South Tibetan detachment in central Nepal during the late Miocene. Opposing both of these interpretations is the view that the Karakoram fault system terminates into the north-south trending Pulan basin [*Ratschbacher et al.*, 1994] or merges and terminates into the Indus-Yalu suture zone in the Mount Kailas area [*Searle*, 1996] (Figure 1). *Murphy et al.* [2002] extended the interpretation of *Ratschbacher et al.* [1994] to include the Gurla Mandhata detachment system, but further concluded that significant right-slip faulting likely extends into the High Himalaya of northwest Nepal. In this paper, we describe a previously unrecognized fault system in the central Himalaya of northwest Nepal that has accommodated tens of kilometers of right-slip motion since the late Miocene. We refer to this fault system as the Gurla Mandhata–Humla fault system (GMH).

2. Geologic Setting

[5] The Himalaya lies between the Indian shield to the south and the Indus-Yalu suture to the north (Figures 1 and 2). In far western Nepal, the first-order geologic framework of the Himalaya consists of four lithotectonic units bounded by four north dipping Cenozoic fault systems: the Main Frontal thrust, the Main Boundary thrust, the Main Central thrust (MCT) zone, and the South Tibet Detachment System (STD) (Figure 2). The Lesser Himalaya is bounded at the base by the Main Boundary thrust and at

the top by the MCT zone and consists of Paleozoic sequences and Mesozoic to early Tertiary strata [*Brookfield*, 1993; *Parrish and Hodges*, 1996; *DeCelles et al.*, 2001]. Other important structures recognized within the Lesser Himalaya include the Ramgarh and Dadeldura thrusts [*Valdiya*, 1981; *Srivastava and Mitra*, 1994; *DeCelles et al.*, 2001; *Pearson*, 2002]. The Greater Himalaya Crystalline Complex is bounded by the MCT zone below and the STD above [*Burg and Chen*, 1984; *Burchfiel et al.*, 1992] and is composed of late Proterozoic to early Cambrian metasedimentary rocks [*Parrish and Hodges*, 1996; *DeCelles et al.*, 2000]. The Tethyan (or north) Himalaya lies between the STD and the Great Counter thrust. It consists of late Precambrian to early Tertiary sedimentary and metasedimentary rocks [*Gansser*, 1964; *Cheng and Xu*, 1987; *Yin et al.*, 1988; *Burchfiel et al.*, 1992; *Brookfield*, 1993; *Garzanti*, 1999]. The entire sequence is referred to as the Tethyan Sedimentary (or metasedimentary) Sequence (TSS). Our study is primarily focused on rocks that are juxtaposed along the MCT zone and STD. These rocks include the Lesser Himalayan sequence (LHS), the Greater Himalayan Crystalline Complex, and the Tethyan Sedimentary Sequence.

[6] The MCT zone in the central Himalaya has had a protracted history. In central Nepal, an early phase of slip is documented from 23 to 20 Ma on the basis of $^{40}Ar/^{39}Ar$ hornblende ages and U-Pb ages of crosscutting leucogranites [*Hubbard and Harrison*, 1989; *Hodges et al.*, 1992, 1996; *Parrish and Hodges*, 1996; *Coleman*, 1996; *Godin et al.*, 2001]. Pliocene Th-Pb ages of monazite inclusions in synkinematic garnets [*Harrison et al.*, 1997, 1998; *Catlos et al.*, 2001, 2002] and $^{40}Ar/^{39}Ar$ muscovite ages [*Macfarlane*, 1993] imply recent exhumation of rocks within the MCT zone. The age of deformation in the MCT zone becomes progressively younger southward and structurally down section, from ~20 Ma at the top to about 5–3 Ma at the base of the MCT zone as Th-Pb ages of monazite inclusions in synkinematic garnets [*Harrison et al.*, 1997, 1998; *Catlos et al.*, 2001, 2002] and $^{40}Ar/^{39}Ar$ muscovite ages [*Macfarlane*, 1993]. In far western Nepal, the MCT zone is interpreted to be active during the early Miocene based on $^{40}Ar/^{39}Ar$ detrital muscovite ages in the Dumri Formation [*DeCelles et al.*, 2001]. In contrast to *Harrison et al.* [1997], *Robinson et al.* [2003] proposed that the MCT did not reactivate at 5–3 Ma but instead was active as a roof thrust to the Lesser Himalayan imbricate thrust system.

[7] Studies along the STD in the central Himalaya indicate that the fault system was active during the middle Miocene [*Edwards and Harrison*, 1997; *Searle et al.*, 1997; *Hodges et al.*, 1996, 1998; *Murphy and Harrison*, 1999]. In the Annapurna-Manslu region of central Nepal, field and geochronologic data demonstrate that this segment of the STD may have been active as recently as the Pleistocene [*Hurtado et al.*, 2001].

[8] In western Tibet the right-slip Karakoram fault system strikes northwest-southeast and cuts across the Shylok suture zone, Banggong-Nujiang suture zone, Shiquanhe ophiolite, and the Great Counter thrust (Figure 1). North of the Mount Kailas area, right-slip estimates along the central segment of the Karakoram fault are 150 to 120 km based on offset of Baltoro-type granite bodies and the Banggong-Nujiang and Shyok suture zones [*Searle*, 1996; *Searle et al.*, 1998; *Phillips et al.*, 2004], and >600 km based on the map pattern of the Indus-Yalu suture zone which suggests large-scale boudinage [*Lacassin et al.*, 2004]. *Phillips et al.* [2004] estimate the central segment of the Karakoram fault to have initiated during the middle Miocene (15.68 ± 0.52 to 13.73 ± 0.28 Ma) based on U-Pb ages of synkinematic plutonic bodies. *Lacassin et al.* [2004] used a similar technique to estimate an earlier initiation between 34 and 23 Ma.

[9] In the Mount Kailas area of southwestern Tibet, a branch of the Karakoram fault system steps southward via the Gurla Mandhata detachment system (Figure 2) [*Murphy et al.*, 2002]. Movement on this detachment system is intimately linked with development of the Gurla Mandhata metamorphic core complex. The maximum fault slip along the Gurla Mandhata detachment system occurs along a pair of low-angle, top-to-west normal faults that have caused significant tectonic denudation of the Tethyan sedimentary sequence, resulting in juxtaposition of weakly metamorphosed Paleozoic rocks and Tertiary sediments in its hanging wall over amphibolite facies mylonitic schist, marble, gneisses, and variably deformed leucogranite bodies in its footwall. Consideration of the original depth of the footwall rocks and dip angle of the detachment fault prior to exhumation of the footwall yields total slip estimates between 66 and 35 km [*Murphy et al.*, 2002]. The footwall rocks can be correlated with the Greater Himalayan Crystalline sequence based on their Sr and Nd isotopic ratios [*Murphy*, 2000]. The $^{40}Ar/^{39}Ar$ data from muscovite and biotite from the footwall rocks indicate that they cooled below <400°C by circa 9 Ma, suggesting that this segment of the Karakoram fault system was active at this time.

[10] On the basis of timing estimates of the MCT zone, STD, and Gurla Mandhata detachment system it is appropriate to ask the following questions: How does the Gurla Mandhata branch of the Karakoram fault system extend across the Himalaya and how does it interact or possibly link with other crustal-scale faults in the Himalaya?

3. Geology of Northwest Nepal

[11] Rocks in northwestern Nepal (Humla district and the northern portion of Bajura district) were mapped during the springs of 2002 and 2003 at a scale of 1:50,000 (Figure 3). The structural framework of the study area may be viewed as consisting of four different components, each with a unique deformational history. They are, the Tethyan fold-thrust belt, the Main Central thrust zone, the Lesser Himalayan imbricate thrust belt, and the Gurla Mandhata–Humla fault system. These structural elements are described below from oldest to youngest.

3.1. Tethyan Fold-Thrust Belt

[12] Exposed in the southwestern portion of the mapped area is a fold-and-thrust system, referred to as the Tethyan

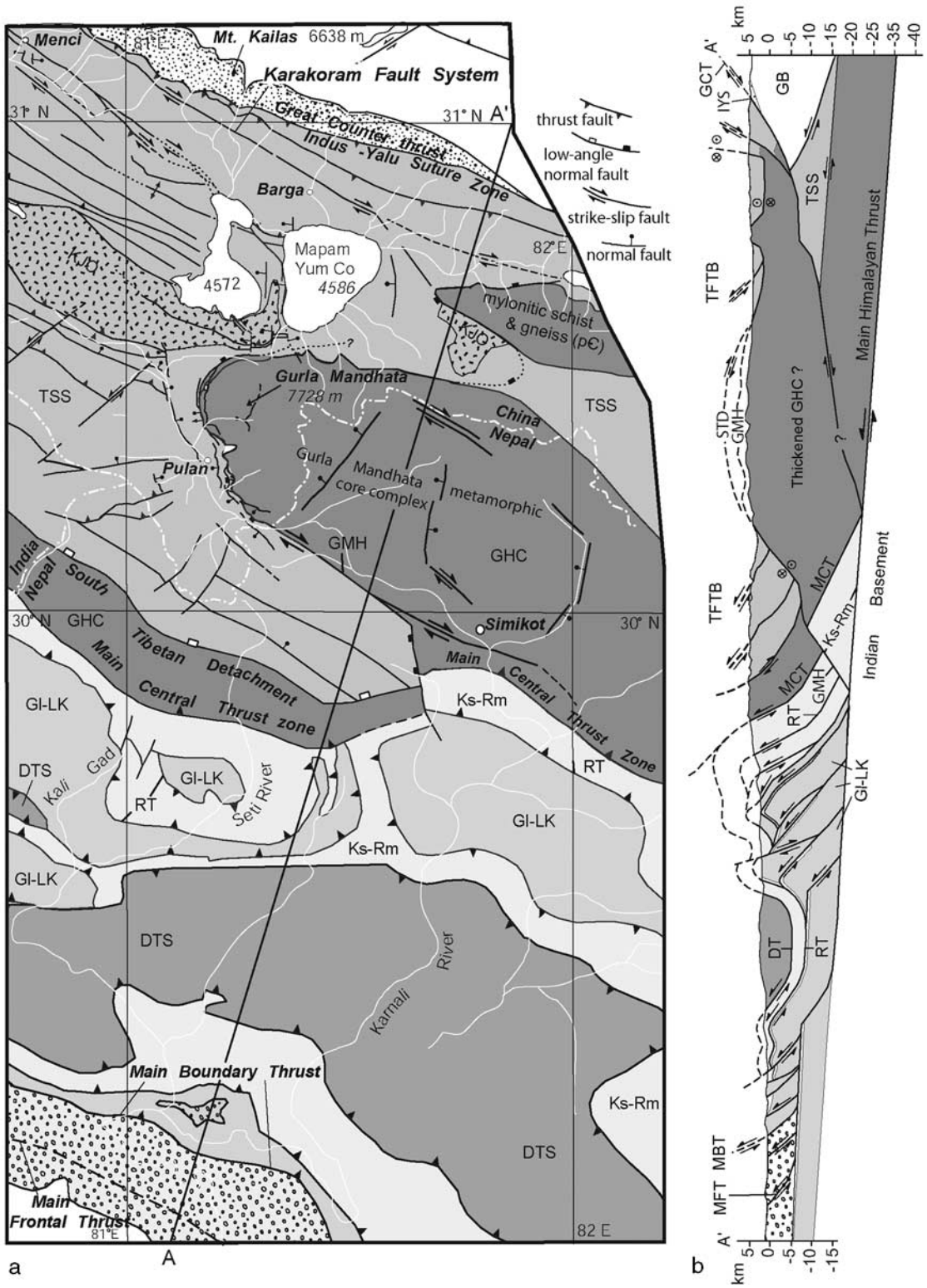
Menci
81°E
Mt. Kailas 6638 m
Karakoram Fault System
Great Counter thrust
Indus -Yalu Suture Zone
31° N
31° N A'
Barga
Mapam Yum Co
4572
4586
82°E
thrust fault
low-angle normal fault
strike-slip fault
normal fault
mylonitic schist & gneiss (pЄ)
Gurla Mandhata 7728 m
China Nepal
TSS
Pulan
Gurla Mandhata core complex
metamorphic GHC
GMH
India Nepal South Tibetan Detachment
30° N GHC
Simikot
30° N
Main Central Thrust zone
Main Central Thrust Zone
Gl-LK
Ks-Rm
RT
DTS
Kali Gad
Seti River
Karnali River
Main Boundary Thrust
Main Frontal Thrust
82 E
a
A
b
GCT
A'
km
5 0 -5 -10 -15 -20 -25 -35 -40
IYS
GB
TSS
TFTB
Main Himalayan Thrust
STD
GMH
Thickened GHC ?
MCT
Ks-Rm
Indian Basement
DT
MBT
MFT
5 0 -5 -10 -15

Figure 2

fold-thrust belt [*Heim and Gansser*, 1939]. It involves a sequence of Cambrian through Mesozoic sedimentary and low-grade metasedimentary rocks. The thickness of the stratigraphic section is uncertain, but may be around 9 km thick based on studies to the northwest [*Cheng and Xu*, 1987; *Murphy and Yin*, 2003]. Within the mapped area, we divide the Tethyan sedimentary series into four units. The stratigraphically lowest unit consists of calcareous paragneisses, phyllites, and metaquartzites. The calcareous rocks contain epidote + quartz + plagioclase + calcite. *Cheng and Xu* [1987] assign a Precambrian age to rocks in southwest Tibet that correlate to this unit. Stratigraphically above is a sequence of interlayered buff quartzite and buff to green phyllite. Bedding has been transposed along south directed bedding parallel shear zones. Crinoid stems of probably Ordovician age are abundant in the phyllitic units [*Cheng and Xu*, 1987].

[13] Folds verge to the south are commonly open to tight and are upright to moderately inclined. They are cylindrical and plunge moderately (5° to 25°) toward the west (Figure 4f). The average orientation of folds calculated from fold axis measurements is 298/10 (Figure 4e).

3.2. Greater Himalayan Complex and Main Central Thrust Zone

[14] The Great Himalayan Complex (GHC) is exposed in the northern region of the mapped area, north of Bogche Gauda (Figure 3). Amphibolite facies metasedimentary schists and gneisses characterize the GHC in the western portion of the study area along the Humla Karnali Nadi. We divide them into three compositionally distinct packages. From structurally lower to higher levels, they are, a pelitic sequence, a carbonate-rich package, and siliceous gneisses and migmatites. The pelitic sequence includes biotite and muscovite schists, quartzfeldspathic gneisses, and metaquartzite gneisses. The carbonate-rich package contains calc-silicate schists and gneisses, biotite and muscovite schists, and quartzofeldspathic gneisses. The structurally highest package is dominated by quartzofeldspathic gneisses, migmatites, and thick (>200 m) tabular discordant and condordant leucogranite plutons.

[15] Peak metamorphic assemblages are preserved in the structurally lowest part of the GHC (near Bogche Gauda). The main phases include kyanite ± garnet ± biotite ± staurolite ± rutile. The first occurrence of sillimanite is at the confluence of Chuwa khola and the Humla Karnali Nadi (Figure 3). Both prismatic and fibrolitic sillimanite is present. Fibrolite is often present along ductile shear surfaces. Calc-silicate rocks of the middle package contain diopside ± hornblende ± biotite ± scapolite + calcite + quartz.

[16] The MCT is marked by a high-strain zone involving the structurally lower portion of the GHC between Dojam and Bogche Gauda in the central portion of the study area (Figure 3). We define the limits of the thrust zone based on the first occurrence of highly strained kyanite-bearing rocks on the south side and the limit of top-to-south contractional shear fabrics on the north side. Using these criteria we estimate the shear zone is ~6 km thick. The density of shear zones within this zone increases toward the base implying the intensity of strain increases toward the bottom (south) of the MCT zone. The average slip direction on faults within the MCT zone is 190° ± 4° (Figure 4g). Fold axes within the MCT zone are isoclinal and trend approximately east-west (92°/11°) (Figure 4g).

3.3. Lesser Himalayan Sequence and Lesser Himalayan Imbricate Thrust Zone

[17] Rocks belonging to the Lesser Himalayan Sequence crop out in the southern portion of the mapped area (Figure 3). Only the stratigraphically lowest units of the LHS were observed in the study area. These include the Kushma and the Ranimata formations (equivalent to the Kuncha Formation. in central Nepal) [*Upreti*, 1999; *DeCelles et al.*, 2001; D. M. Robinson, personal communication, 2003]. The Kushma Formation crops out immediately below the MCT zone and repeated by a thrust to the south (Figure 3, cross section D–D″). It is >1 km thick and is characterized by white to tan, metaquartzite containing thin (~1–2 mm) seams of biotite. The Ranimata Formation is internally shortened by south directed thrusts. It is >3.5 km thick and is characterized by interlayered garnet-bearing chloritic schist and biotite schist, with minor amounts of 1- to 2-m-thick amphibolite layers and marble. Within the Ranimata Formation is a >150-m-thick quartzofeldspathic augen gneiss that can be correlated with the Ulleri gneiss in central Nepal [*DeCelles et al.*, 2001]. Along the Humla Karnali Nadi and immediately north of the village of Chyachaur the Ulleri gneiss is mylonitic. The degree of penetrative deformation within it is variable along strike.

[18] The northern portion of the Lesser Himalayan imbricate thrust zone [*DeCelles et al.*, 2001] extends across the southern part of the study area (Figure 3). Several south directed imbricate thrusts were identified within the LHS. The average slip direction on these imbricate thrust faults is 199° ± 3° (Figure 4h). Shear zones within the Ulleri gneiss

Figure 2. (a) Regional geologic map of southwest Tibet and northwestern Nepal compiled from *Heim and Gansser* [1939], *Valdiya* [1981], *Cheng and Xu* [1987], *Shrestha et al.* [1987], *DeCelles et al.* [1998], *DeCelles et al.* [2001], *Yin et al.* [1999], and *Murphy et al.* [2002]. Abbreviations are DTS, Dadeldhura thrust sheet; GHS, Greater Himalayan sequence; Gl-LK, Galyang-Lakharpata formations; KJO, Kiogar-Jungbwa ophiolitic and mantle-type rocks; Ks-Rm, Kushma-Ranimata formations; RT, Ramgarh thrust; TSS, Tethyan Sedimentary Sequence. Rivers are shown as white line, and international border is shown as white dash-dotted line. (b) Regional cross section across the Himalaya on the basis of published profiles of *DeCelles et al.* [2001], *Murphy and Yin* [2003], and this study. Additional abbreviations are GB, Gangdese batholith; GCT, Great Counter thrust; IYS, Indus-Yalu suture zone; TFTB, Tethyan fold-thrust belt.

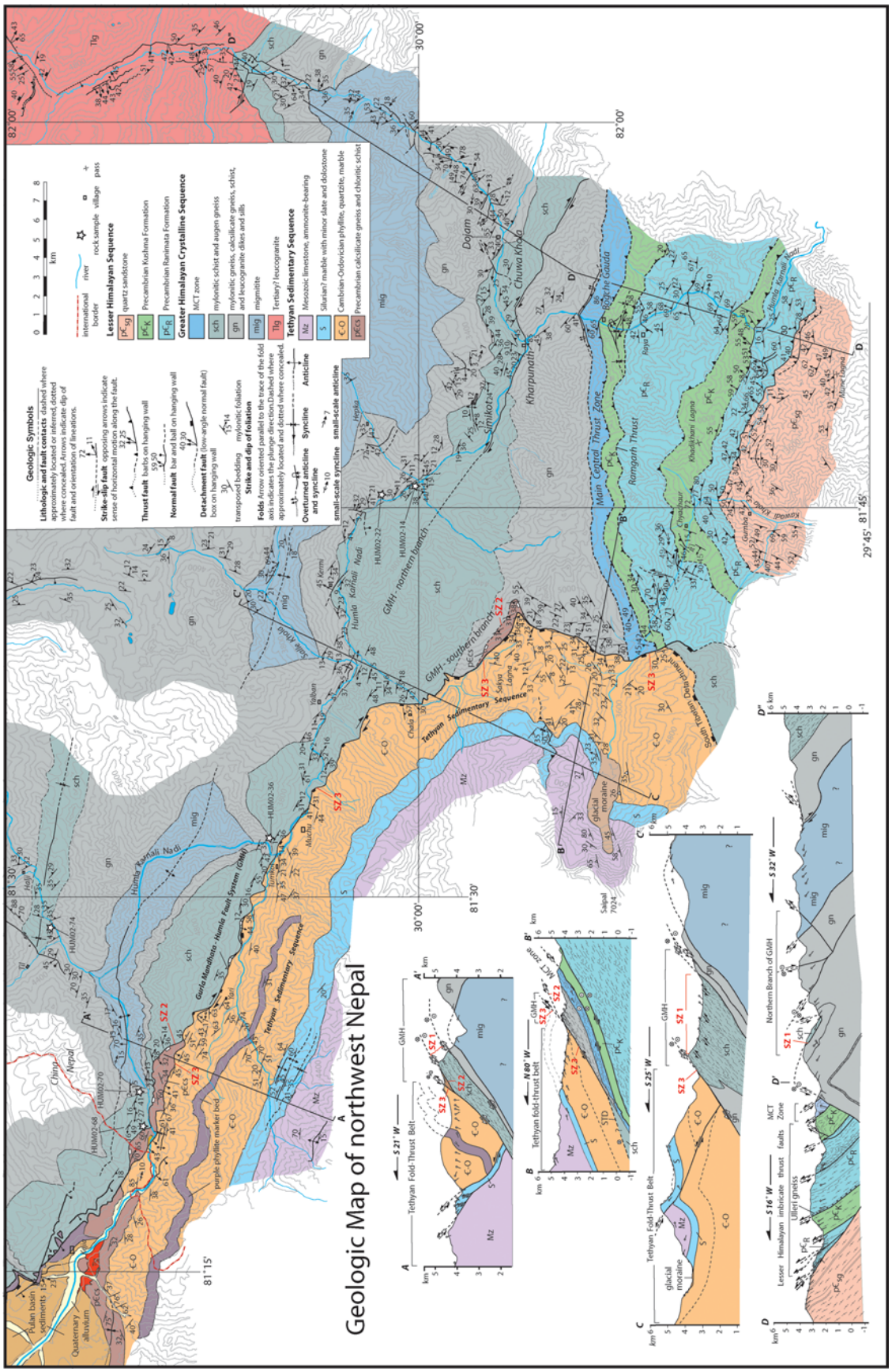

Figure 3. Geologic map and cross sections through Humla and Bajura districts in northwest Nepal. Topographic base map is from Nepal Survey Department.

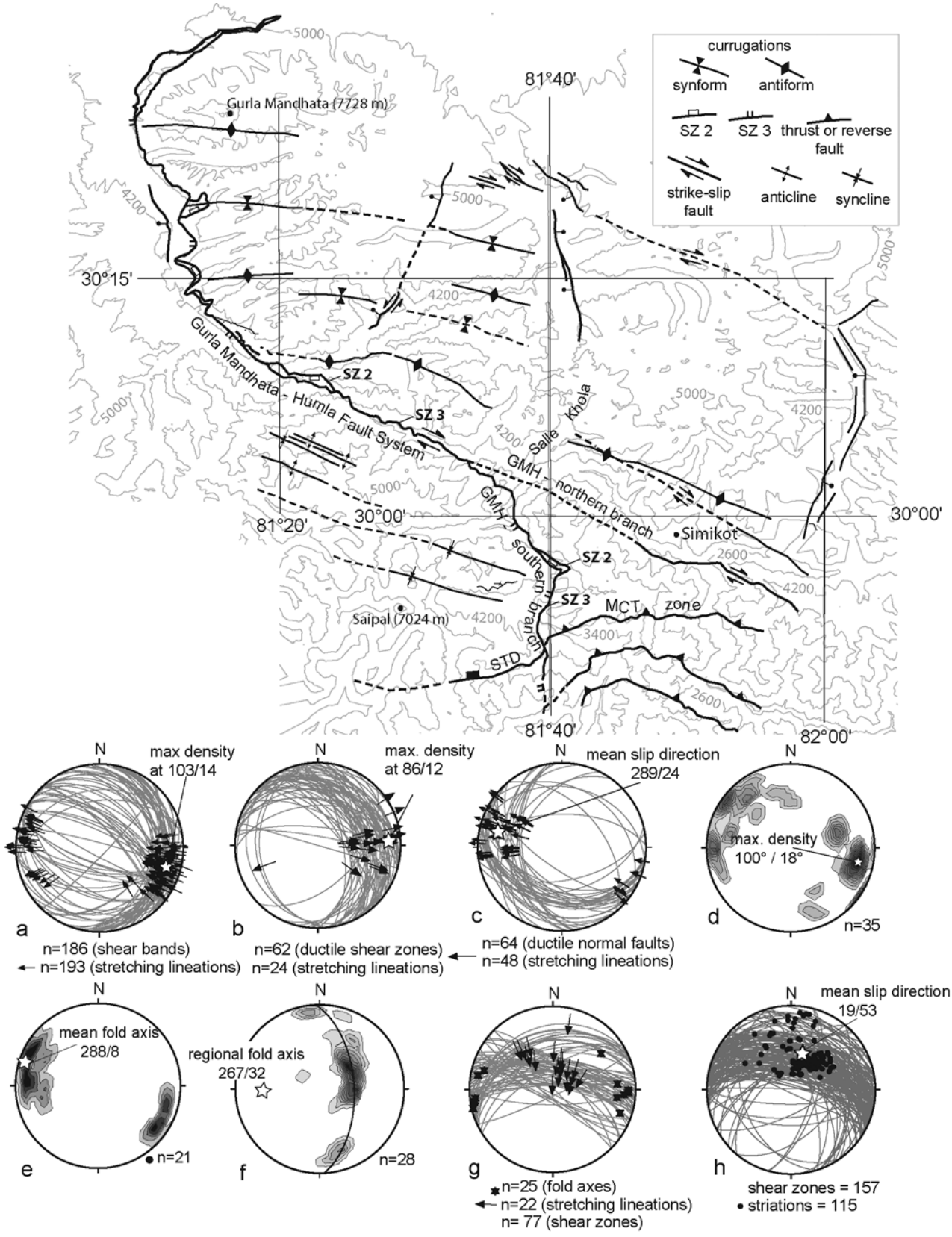
currugations
synform
antiform
SZ 2
SZ 3
thrust or reverse fault
strike-slip fault
anticline
syncline
Gurla Mandhata (7728 m)
81°40'
30°15'
30°00'
81°20'
82°00'
Gurla Mandhata - Humla Fault System
SZ 2
SZ 3
Sale Khola
GMH - northern branch
GMH - southern branch
Simikot
MCT zone
STD
Saipal (7024 m)
5000
4200
3400
2600
a
max density at 103/14
n=186 (shear bands)
n=193 (stretching lineations)
b
max. density at 86/12
n=62 (ductile shear zones)
n=24 (stretching lineations)
c
mean slip direction 289/24
n=64 (ductile normal faults)
n=48 (stretching lineations)
d
max. density 100° / 18°
n=35
e
mean fold axis 288/8
n=21
f
regional fold axis 267/32
n=28
g
n=25 (fold axes)
n=22 (stretching lineations)
n= 77 (shear zones)
h
mean slip direction 19/53
shear zones = 157
striations = 115

Figure 4

are steeply dipping to the northeast and the sense of shear is west-southwest.

3.4. The Gurla Mandhata–Humla Fault System

[19] Development of the GMH postdates movement on all structures described above. On the basis of field mapping and structural analysis, we identified three shear zones that play key roles in its structural evolution (Figure 3). Collectively, we refer to these three shear zones as the GMH. These shear zones and the rock units they involve are discussed below from lower to higher structural levels and are referred to as shear zone 1 (SZ 1), shear zone 2 (SZ 2), and shear zone 3 (SZ 3).

[20] The oldest shear zone, SZ 1 is a broadly folded, south dipping ductile shear zone that strikes WNW-ESE across the study area (Figure 3). It cuts across the garnet-biotite-muscovite schists (sch) and muscovite-biotite quartz-ofeldspathic gneisses (gn) (Figure 3). Structurally below SZ 1 is a domed migmatite unit. The migmatite consists of leucocratic bodies (elliptical bodies ~0.2–3 m in diameter and dikes up to 2 m thick), biotite-rich zones, and banded gneiss that contain an isoclinally folded mylonitic fabric. The characteristic mineral assemblage of the shear zone rocks is (bt + ms + grt + plg + sil). Several fabric elements in outcrop and thin sections oriented parallel to lineation show asymmetry (asymmetric biotite and muscovite grains [mica fish], stair-stepped feldspar grains and porphyroclasts, S/C/C′ foliations, and stair-stepped boudins of leucogranite sills) indicating a significant simple shear component of deformation of the footwall. S/C/C′ foliations are defined by aligned biotite and muscovite clusters, recrystallized quartz bands (quartz ribbons) and alignment of feldspar porphyroclasts (Figure 5a). Some layers within the shear zone fabric are dominated by discrete lineations composed primarily of clasts of quartz and feldspar aggregates indicating constrictional deformation conditions existed during the evolution of the SZ 1. Feldspar porphyroclasts are mantled by recrystallized feldspar suggesting the temperature of deformation was 400–500°C [*Tullis and Yund*, 1991]. Stretched tourmaline grains within SZ 1 yield extension values of 20–30% toward the WNW-ESE. Shear sense indicators show a change in the sense of shear along strike. In the western portion of the study area, (west of Salle Khola, Figure 3) the sense of shear is dominantly top-to-west (Figure 4a). In the eastern portion of the study area, along Chuwa Khola, the sense of shear is dominantly top to east. In the eastern portion of the study area, these east-west shear sense indicators abut top-to-south deformation fabrics that are a part of the MCT zone (Figure 4b). Over a structural distance of ~1 km, between Kharpunath and Dojam (Figure 3) east-west shear sense indicators overprint top-to-south fabrics.

[21] Subhedral to anhedral garnet contains a nonrotational growth history and normally do not preserve a foliation within their interiors. Th-Pb dating of monazite inclusions in garnets from rocks that correlate to these rocks suggests garnet growth occurred between 16 and 10 Ma [*Murphy et al.*, 2002].

[22] In map view, the surface exposure of SZ 1 occupies a region with dimensions of ~100 km in a northwest-southeast direction and 40 km in a northeast-southwest direction. Within this region, SZ 1 is folded into a series of doubly plunging, upright antiforms and synforms that we refer to as corrugations (Figure 4). Their wavelength is ~10 km and trend subparallel to the SZ 1stretching lineation (Figure 4d). We interpret these folds formed coeval with slip along SZ 1 and prior to initiation of the overlying younger shear zone, SZ 2, since SZ 1 is more folded than SZ 2.

[23] SZ 2 is a south dipping ductile shear zone that extends WNW-ESE across the study area (Figure 3). It juxtaposes Precambrian calc-silicate rocks in its hanging wall against mylonitic schists and gneisses in its footwall. It is a high strain zone that lies structurally above and cross-cuts SZ 1 at a 5–15° angle. Shear sense indicators include S/C/C′ fabrics, ductile normal faults, and asymmetric mica grains. S/C/C′ fabrics are defined by aligned biotite, muscovite, and recrystallized quartz. Feldspar grains are angular and variable in size (Figure 5b). Locally, feldspar grains show domino-style tilting. The SZ 2 stretching lineation is defined by aligned biotite and muscovite clusters and recrystallized quartz. Nearly all shear sense indicators show top-to-the-west sense of shear. Contoured stretching lineations show a maximum density at 289/24 (Figure 4c). The spatial extent of these fabrics defines a 0.5- to 2-m-thick shear zone.

[24] SZ 3 is a brittle south dipping fault zone that extends WNW-ESE across the study area. It locally incises SZ 2 and SZ 1 (Figures 3 and 6). SZ 3 juxtaposes Cambrian-Ordovician phyllites and metaquartzites in its hanging wall against calc-silicate rocks in its footwall. The hanging wall rocks primarily record north-south contractional deformation that we interpret to be related to the Tethyan fold-thrust belt. Adjacent to the SZ 3, these contractional structures are overprinted by brittle right-slip faults, normal faults, and

Figure 4. Structure map of northwestern Nepal and its neighboring Tibetan areas based on geologic mapping and interpretation of ASTER data. GMH is composed of SZ 1, SZ 2, and SZ 3. See text for explanation. (a) Stereoplot of SZ 1 shear bands and stretching lineations west of Salle Khola. Arrow indicates slip direction of hanging wall. (b) Stereoplot SZ 2 shear bands and stretching lineations east of Salle Khola. (c) Stereoplot of SZ 2 shear bands and stretching lineations. (d) Contoured fold axis measurements within the Gurla Mandhata metamorphic core complex. (e) Stereoplot of fold axes in Tethyan Sedimentary Sequence with contours at 3, 7, 11, and 15. (f) A π diagram of foliations in Tethyan Sedimentary Sequence with contours at 3, 7, 11, and 15. (g) Stereoplot of shear zones, striations, and fold axes within the Main Central thrust zone. (h) Stereoplot of shear zones and striations within the Lesser Himalayan imbricate thrust zone. All stereonets are lower hemisphere, equal-area. Topographic base is derived from Shuttle Radar Topography Mission data. Contour interval is 800 m.

joints that strike subparallel to the main trace of SZ 3. We correlate the footwall rocks with Precambrian rocks exposed in southwest Tibet based on lithology [*Cheng and Xu*, 1987]. Cataclastic deformation penetrates 2–5 m beneath SZ 3. One to three centimeter thick layers of brecciated mylonitic rock lie subparallel to mylonitic foliation. These brecciated layers are cross cut by epidote-, chorite-, and quartz-filled conjugate shear fractures that strike parallel to the mylonitic foliation. The mean orientation of SZ 3 striations is 280°/20°.

[25] SZ 2 and SZ 3 branch in the central portion of the study area. The northern branch strikes east–west and passes through the village of Simikot (Figure 4). The southern branch strikes north-south, forming a major right-stepping extensional bend in the GMH. SZ 2 and SZ 3 follow the southern branch. Both the MCT zone and the STD are cut by the southern branch of the GMH (Figure 3). *DeCelles et al.* [2001] locate the MCT ~10 km south of our mapped MCT on the east side of the GMH, indicating an apparent left lateral separation caused by top-to-west normal faulting.

[26] Variably deformed leucogranite bodies make up ~5% to 10% of the rock within SZ 1. Five lithologic units were recognized: (1) muscovite granite, (2) tourmaline-muscovite granite, (3) muscovite-biotite granite, (4) biotite granite, and (5) biotite-garnet granite. We use the term granite to describe leucocratic (qtz + K-feldspar + plg) rocks in general. The most abundant rock is tourmaline-muscovite bearing granite. Leucogranite bodies occur primarily as dikes and sills that are tens of centimeters to 20 m thick. They generally display sharp contacts with the country rock. There are at least two generations of dikes/sills based on our field observations. The older set parallels the foliation and displays a mylonitic foliation subparallel to that in the country rock. In the eastern part of the field area, we observed a large leucogranite body (Figure 3). It is undeformed to weakly foliated. The contact between the granite body and the country rock is sheared subparallel to the shear sense direction within the SZ 1, indicating emplacement occurred prior to or contemporaneous with the development of the shear zone.

[27] Th-Pb dating of monazite from eight leucogranite bodies was conducted using the Cameca 1270 ion microprobe at UCLA (Table 1). All samples were collected within SZ 1. 5 undeformed leucogranite dikes (HUM02-22, HUM02-70, HUM02-74, HUM02-85, HUM02-90) and 3 deformed leucogranite sills (HUM02-14, HUM02-36, HUM02-68) were dated (Table 1). All undeformed leucogranite bodies are cut by brittle structures that we associate

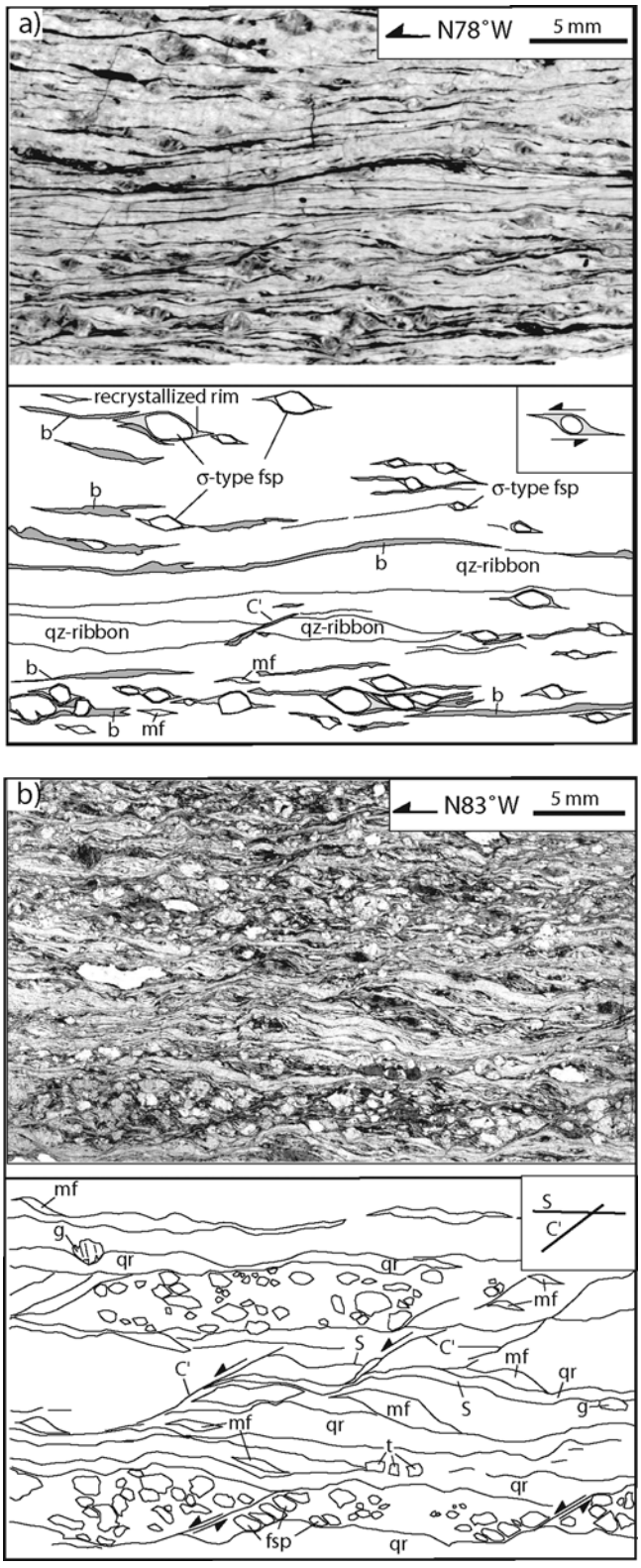

Figure 5. Photomicrographs of rocks within GMH. Sections are parallel to stretching lineation and normal to foliation. PPL. (a) Mylonitic micashist within SZ 1. Feldspar porphyroclasts are stair stepped and mantled by recrystallized feldspar. Feldspar porphyroclasts and mica fish indicate top-to-west shear sense. (b) C′-type shear band transecting S-type foliation in a mylonitic biotite schist within SZ 2. S/C′ foliations and mica fish indicate show top-to-west shear sense. Stretched tourmaline grain indicates approximately E-W extension. Feldspar grains show brittle behavior. Abbreviations are b, biotite grain(s); fsp, feldspar grain(s); g, garnet; mf, mica fish; qr, quartz ribbon, S, S-type shear band; C′, C′-type shear band.

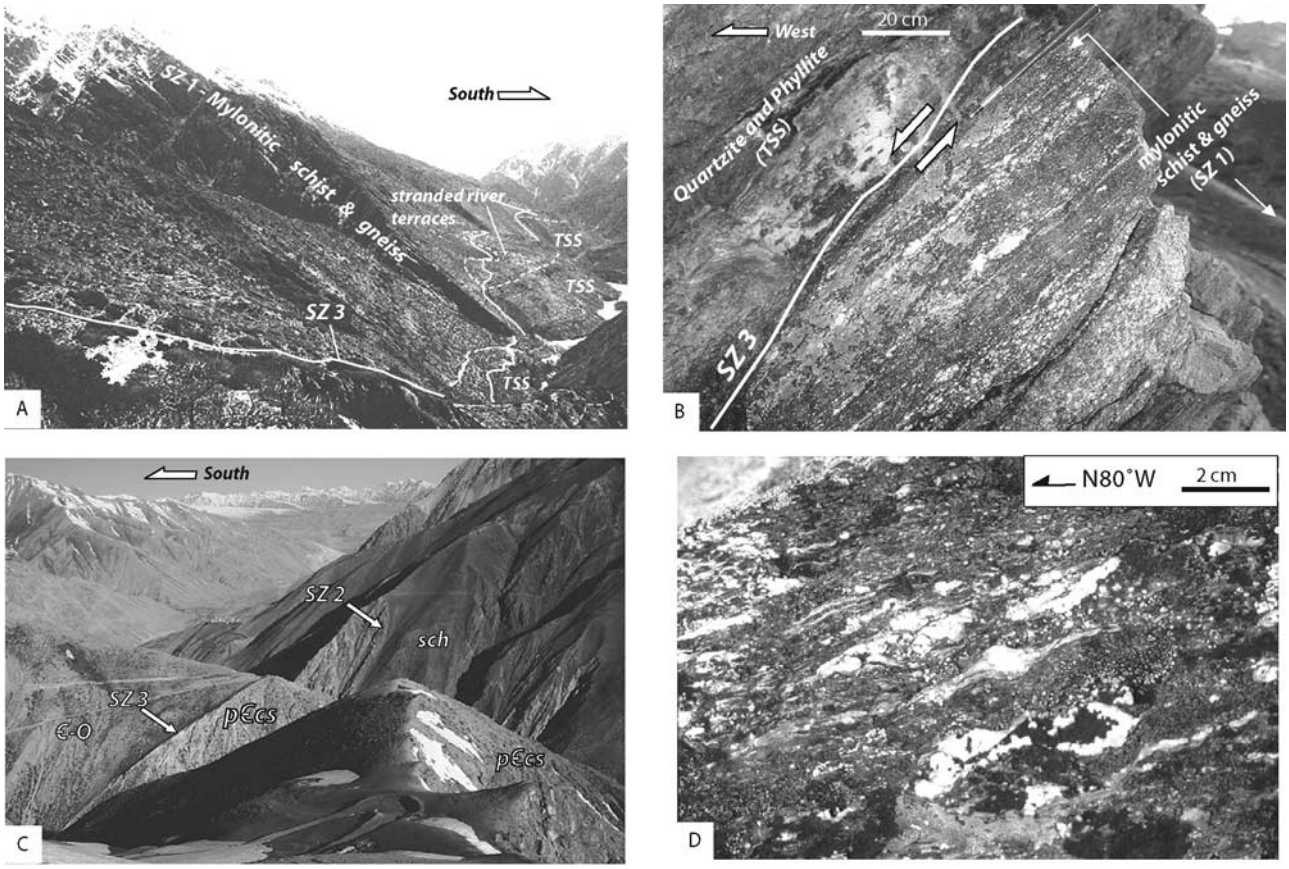

Figure 6. Photographs of the Gurla Mandhata-Humla fault system (GMH). (a) View to east near the village of Tumkot in the NW part of the study area (Figure 3). The relief between the high peaks on the left and the river valley on the right is ~800 m. Abbreviations are TSS, Tethyan Sedimentary Sequence. (b) GMH, view to the north near Sakya Lagna in SW part of the study area (Figure 3). GMH is typified by a sharp contact between phyllites and quartzites that belong to the TSS juxtaposed against mylonitic schists and gneisses that belong to the GHC. (c) GMH at the Nepal-China border, view to the west. (d) Mylonitic micaschist within SZ 1. Sigmoidally shaped feldspar porphyoclast with recrystallized rim indicate top-west shear sense.

with motion along SZ 3. We obtained $^{208}Pb/^{232}Th$ ion microprobe monazite ages following the method described by *Harrison et al.* [1995]. Approximately 20 grains of monazite were separated from a 1 kg rock sample using standard rock crushing and mineral separation techniques and were mounted in epoxy with a monazite standard (554) and Au coated. Between 4 and 15 monazite grains were analyzed from each sample; a single spot was analyzed in most grains; two grains were analyzed in two spots with excellent reproducibility on the duplicate analyses.

[28] The weighted means of the monazite ages from individual samples ranges from 9.29 ± 0.09 to 14.79 ± 0.06 Ma. The weighted average of deformed samples ranges from 14.8 to 10.8 Ma and undeformed samples range in age from 13.2 to 9.3 Ma. Given the number of points we have from each sample it is not completely clear if the ages represent analytical error around a central value (the crystallization age) or if the spread in ages in an individual sample represents a crystallization age with variable amounts of Pb loss or inheritance. Given the age of these samples, the relatively high closure temperature of Pb in monazite [*Copeland et al.*, 1990; *Parrish*, 1990], and the temperature of peak metamorphism of the surrounding rocks, we discount the possibility of significant Pb loss. However, if inherited Pb is present in these monazites then the youngest ages obtained may be a better estimate of the crystallization age of these granites than the weighted average (Figure 7). In that case, the undeformed rocks span from 7.0 to 12.4 Ma and the deformed samples range in age from 7.0 to 13.6 Ma. It seems the case for inheritance is strongest for samples 14, 70 and 90 and weakest for sample 36. Regardless of how we interpret the crystallization age of these granitic dikes there is little correlation between the degree of deformation of the dikes and their age. Moreover, these data indicate anatexis and

Table 1. The $^{232}Th/^{208}Pb$ Ion Microprobe Monazite Ages From Leucogranite Bodies Within SZ 1[a]

Sample	$^{208}Pb^*/^{232}Th$	±1 SE	Age, Ma	±1 SE	$^{208}Pb^*$, %
HUM02-14-01-01	0.000355	0.000007	7.18	0.14	93.4
HUM02-14-03-01	0.000639	0.000014	12.91	0.28	93.8
HUM02-14-05-01	0.002239	0.000824	*45.19*	*16.60*	*9.0*
HUM02-14-07-01	0.000572	0.000016	11.55	0.32	92.9
HUM02-14-09-01	0.000733	0.000009	14.82	0.18	95.2
HUM02-14-09-02	0.000585	0.000013	11.83	0.26	93.3
HUM02-14-11-01	0.000632	0.000019	12.76	0.38	86.1
HUM02-14-13-01	0.007705	0.013400	*155.10*	*268.00*	*99.5*
HUM02-14-14-01	0.000620	0.000011	12.52	0.23	92.5
HUM02-14-15-01	0.000636	0.000011	12.84	0.21	91.7
HUM02-14-17-01	0.000644	0.000014	13.01	0.29	92.0
HUM02-14-18-01	0.000348	0.000011	7.04	0.22	85.3
HUM02-14-18-02	0.000378	0.000009	7.64	0.18	88.4
HUM02-14-19-01	−0.017250	0.081500	*−351.60*	*1680.00*	*99.6*
HUM02-14-21-01	0.000593	0.000008	11.99	0.17	91.4
HUM02-14-22-01	0.000616	0.000012	12.44	0.23	92.2
Weighted mean ±1 SE			11.54	0.07	
HUM02-22-01-01	0.000629	0.000018	12.71	0.36	93.4
HUM02-22-03-01	0.000593	0.000009	11.98	0.19	93.4
HUM02-22-12-01	0.000836	0.000037	16.88	0.75	17.3
HUM02-22-13-01	0.001216	0.000347	24.55	7.00	97.7
HUM02-22-14-01	0.000637	0.000018	12.87	0.36	72.1
HUM02-22-19-01	0.000577	0.000011	11.65	0.22	82.5
HUM02-22-19-02	0.000593	0.000018	11.99	0.36	83.6
Weighted mean ±1 SE			12.17	0.12	
HUM02-36-06-01	0.000673	0.000032	13.59	0.64	83.0
HUM02-36-07-01	0.000742	0.000009	14.99	0.18	95.4
HUM02-36-08-01	0.000740	0.000009	14.95	0.18	94.3
HUM02-36-10-01	0.000740	0.000009	14.95	0.18	96.0
HUM02-36-11-01	0.000737	0.000008	14.90	0.16	94.8
HUM02-36-12-01	0.000733	0.000009	14.82	0.18	95.2
HUM02-36-14-01	0.000695	0.000008	14.04	0.16	94.5
HUM02-36-15-01	0.000730	0.000009	14.75	0.18	88.5
HUM02-36-16-01	0.000749	0.000009	15.13	0.17	94.1
Weighted mean ±1 SE			14.79	0.06	
HUM02-68-01-01	0.000563	0.000009	11.38	0.19	92.5
HUM02-68-02-01	0.000598	0.000011	12.08	0.21	94.7
HUM02-68-08-01	0.000586	0.000011	11.83	0.22	87.4
HUM02-68-13-01	0.000613	0.000008	12.39	0.17	95.4
HUM02-68-16-01	0.000586	0.000022	11.85	0.45	82.4
HUM02-68-18-01	0.000551	0.000008	11.14	0.17	95.1
HUM02-68-22-01	0.000578	0.000011	11.69	0.23	96.0
Weighted mean ±1 SE			11.74	0.08	
HUM02-74-01-01	0.000524	0.000011	10.60	0.21	92.5
HUM02-74-03-01	0.000538	0.000012	10.87	0.24	92.8
HUM02-74-04-01	0.000596	0.000011	12.04	0.21	95.2
HUM02-74-05-01	0.000571	0.000011	11.53	0.21	89.9
HUM02-74-06-01	0.000534	0.000013	10.80	0.26	92.9
HUM02-74-07-01	0.000575	0.000008	11.61	0.16	91.0
HUM02-74-08-01	0.000578	0.000012	11.67	0.24	93.8
Weighted mean ±1 SE			11.36	0.08	
HUM02-85-01-01	0.000731	0.000042	14.77	0.84	64.0
HUM02-85-01-01	0.000775	0.000095	15.66	1.91	89.6
HUM02-85-12-01	0.000685	0.000032	13.85	0.66	93.7
HUM02-85-13-01	0.000800	0.000086	16.17	1.73	29.4
HUM02-85-14-01	0.000614	0.000016	12.40	0.33	85.0
HUM02-85-15-01	0.000650	0.000017	13.13	0.35	87.7
HUM02-85-18-01	0.000739	0.000035	14.94	0.70	38.2
HUM02-85-19-01	0.000659	0.000017	13.32	0.34	87.0
HUM02-85-20-01	0.000641	0.000020	12.95	0.40	76.9
Weighted mean ±1 SE			13.21	0.16	
HUM02-90-02-01	0.000630	0.000039	12.72	0.78	88.6
HUM02-90-03-01	0.000721	0.000024	14.57	0.49	92.8
HUM02-90-04-01	0.000524	0.000039	10.58	0.80	81.6
HUM02-90-13-01	0.000503	0.000030	10.16	0.62	90.2
HUM02-90-15-01	0.000464	0.000006	9.39	0.11	99.4
HUM02-90-17-01	0.001326	0.000181	*26.78*	*3.65*	*37.6*
HUM02-90-18-01	0.000635	0.000068	12.83	1.37	58.4
Weighted mean ±1 SE			9.78	0.11	
HUM02-70-01-01	0.000567	0.000009	11.46	0.19	92.5
HUM02-70-06-01	0.000516	0.000012	10.42	0.25	90.2
HUM02-70-07-01	0.000538	0.000011	10.87	0.23	90.7
HUM02-70-12-01	0.000413	0.000020	8.35	0.41	70.8
HUM02-70-16-01	0.000344	0.000007	6.95	0.15	89.0
Weighted mean ±1 SE			9.29	0.09	

[a]Grains in italics were not used in calculations of weighted means. For all samples the following values were used to correct for common Pb: $^{206}Pb/^{204}Pb$ = 18.7; $^{207}Pb/^{204}Pb$ = 15.63; $^{208}Pb/^{204}Pb$ = 37.86. Sample nomenclature: HUM02-XX-YY-ZZ; XX is the sample number, YY is the number of the monazite grain from that sample, ZZ is the number of the analysis from that grain.

deformation of the region was ongoing over the time from at least 14 to 9 Ma and perhaps as long as 15 to 7 Ma.

4. Evolution of the Gurla Mandhata–Humla Fault System

4.1. Magnitude of Slip

[29] We estimate the net slip on the southern branch of the GMH by restoring the MCT zone across the fault system (Figure 2). We make three general assumptions in our restoration. (1) The total offset of the MCT zone solely results from movement along the GMH fault system. (2) The GMH fault system has maintained a constant slip direction throughout its evolution. (3) The MCT zone was planar and continuous across far western Nepal prior to slip on the GMH fault system.

[30] The geometric relationship between the MCT zone and the GMH on the east side of the GMH was determined by our field mapping. We interpret the geometric relationship on the west side of the GMH based on field mapping by *DeCelles et al.* [2001] and analysis of ASTER (Advanced Spaceborne Thermal Emission and Reflection Radiometer) images. The best fit plane to shear zone measurements within the MCT zone on the east side of the fault is N76°W/45°NE. We assume the MCT zone on the west side of the GMH has the same orientation. The mean orientation of the southern branch of the GMH where it intersects with the MCT zone is N18°E/34°NW. We restore the MCT zone in a direction parallel to the mean slip direction of N87°W on the GMH. Using this method we estimate 21 km of net slip on the southern branch of the GMH.

[31] We have not identified offset markers along the northern branch of the GMH. However, we estimate extension across the shear zone using sheared leucogranite dikes that are discordant to SZ 1 shear fabrics. We interpret

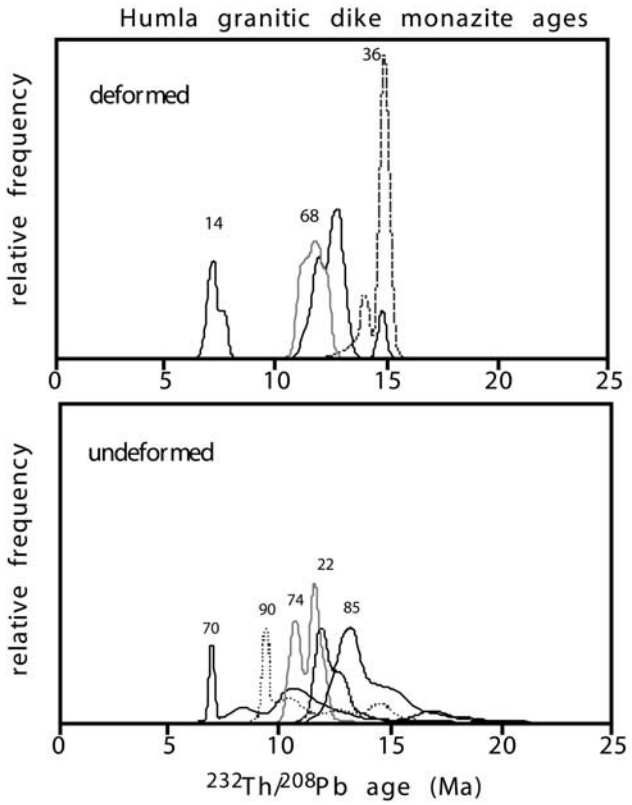

Figure 7. Relative probability diagrams for $^{232}Th/^{208}Pb$ ages for monazites from granitic dikes and sills. Numerals above youngest peak for each curve indicate sample numbers.

shearing of these dikes occurred during late stage movements along SZ 1 since they are sheared in a direction parallel to the slip direction of SZ 1. Shear angles of deformed dikes are high and vary between 60 and 80° yielding shear strains between 1.7 and 5.7. Applying this estimate to the entire width of the northern branch of the GMH, 2 km, yields 11.4 to 3.4 km of right-lateral shear. This is a minimum slip estimate for SZ 1 since the dikes intruded the shear zone after some unknown amount of shear.

4.2. Structural Model

[32] Two results have chiefly motivated construction of the structural model described below (Figure 8): (1) The MCT zone, which has accommodated a significant amount of the total shortening in the Himalaya, is cut by the GMH, and the latter has accommodated tens of kilometers of arc-parallel extension; and (2) the time of high-grade metamorphism related to burial/crustal thickening is only a few million years older than arc-parallel extension accommodated by the GMH.

[33] Figure 8a shows the structural setting from the late Oligocene to middle Miocene prior to initiation of the GMH fault system. During this period south directed and north directed contractional structures result in horizontal shortening and vertical thickening of rocks later exhumed by the GMH and exposed within the Gurla Mandhata metamorphic core complex. Horizontal shortening of the GHC and LHS occurs by movement on south directed contractional structures, including the MCT zone, Dadeldhura thrust, and the Ramgarh thrust that have initiated from north to south toward the foreland, respectively [*DeCelles et al.*, 2001; *Pearson*, 2002]. North directed thrusting occurs along the Great Counter thrust [*Heim and Gansser*, 1939; *Gansser*, 1964; *Yin et al.*, 1999]. Our regional cross section across the Himalaya (Figure 2b) requires 100% crustal thickening beneath the Gurla Mandhata metamorphic core complex. We suggest that this crustal thickening was accomplished by stacking the GHC over the TSS along north directed thrusts possible related to the GCT as has been previously proposed for other gneiss domes immediately south of the Indus-Yalu suture [*Makovsky et al.*, 1999; *Lee et al.*, 2000; *Yin*, 2005], collectively referred to as the north Himalayan gneiss domes. Structural models explaining their development call upon south directed [*Valdiya*, 1989; *Hauck et al.*, 1998] and north directed thrusting [*Makovsky et al.*, 1999; *Lee et al.*, 2000; *Yin and Harrison*, 2000]. Although our study of the GMH and Gurla Mandhata metamorphic core complex requires east-west stretching to play a role in its development, we cannot rule out an earlier deformation phase dominated by north-south shortening. Th-Pb dating of monazite inclusions in garnets from SZ 1 rocks suggests these rocks were buried during the middle Miocene [*Murphy et al.*, 2002]. Petrographic data from early Miocene foreland basin deposits (Dumri Formation) suggest its source terrane is the GHC [*DeCelles et al.*, 1998]. The $^{40}Ar/^{39}Ar$ ages from detrital muscovites in Dumri Formation indicate that its source terrane cooled below 350°C at ~20 Ma [*DeCelles et al.*, 2001]. *DeCelles et al.* [2001] interpret this cooling event to be associated with emplacement of the Main Central thrust sheet.

[34] Figure 8b shows the development of the GMH fault system and related exhumation of the Gurla Mandhata metamorphic core complex. These structures form in the region of thickened crust between the MCT zone and GCT. The GMH extends southeast across northwest Nepal via east-west striking segments (right-slip faults) and north-south striking segments (normal faults) (Figure 3). Movement along the GMH results in left-lateral separation of the Lesser Himalayan imbricate thrust zone, MCT zone, and STD.

[35] For ~50 km along strike in the western portion of the study area the GMH juxtaposes Cambrian-Orodovician age phyllitic rocks against GHC. Because this is the same lithologic relationship observed across the STD in the central Himalaya, we interpret this segment of the GMH to root into the same structural position as the STD. This implies that the geometry of the GMH approximates that of the STD (Figure 2a). In our model, growth of the Gurla Mandhata metamorphic core complex results from contemporaneous east-west extension and north-south shortening. East-west extension is accommodated by top-to-west shear along the northwestern step over and an inferred top-to-the-east shear zone on the eastside of the dome, resulting in the evolution of the Gurla Mandhata metamorphic core com-

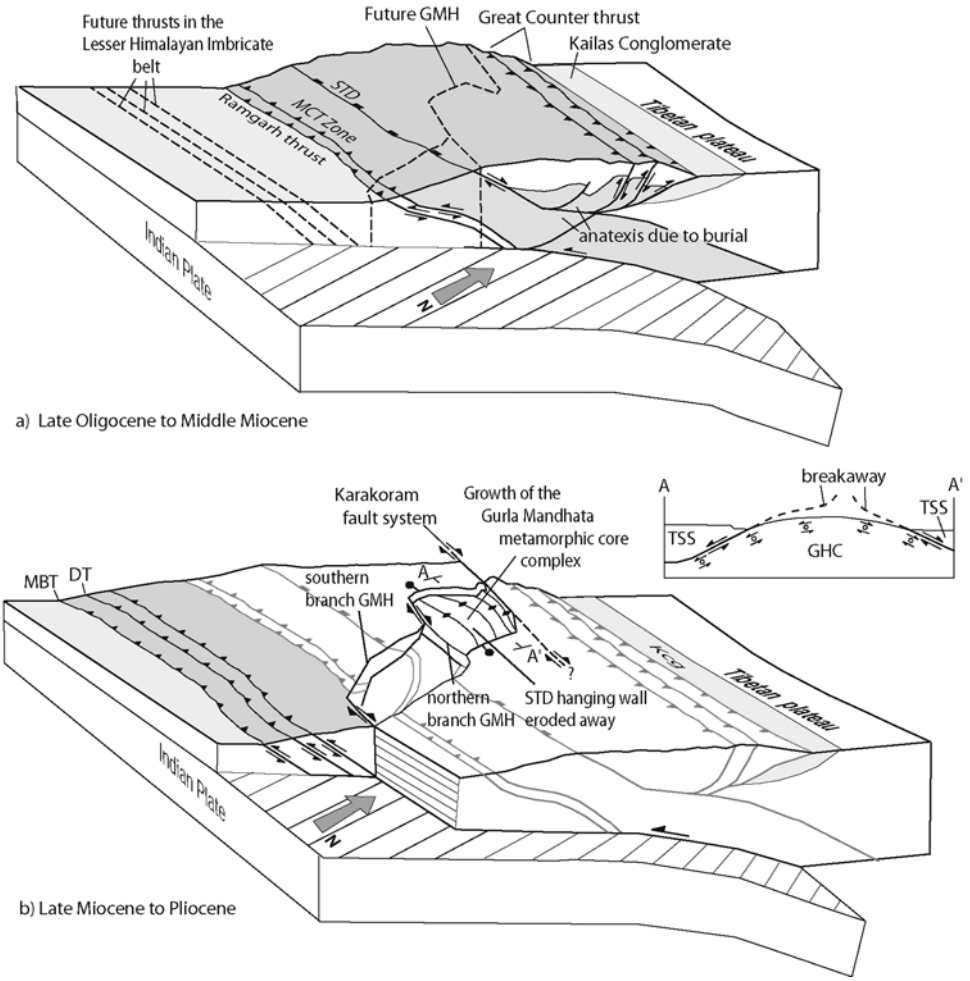

Figure 8. Structural model showing evolution of Himalayan convergent margin in far western Nepal since the early Miocene. See text for explanation. (a). Early to middle Miocene geologic setting characterized by crustal thickening in region between MCT and Indus-Yalu suture zone. (b). Middle Miocene to Recent geologic setting characterized by initiation of GMH in region previously thickened in earlier stage. Schematic profile A–A′ illustrates the bivergent nature of the extension direction across the Gurla Mandhata metamorphic core complex. Abbreviations are DT, Dadeldhura thrust; GHC, Greater Himalayan Complex sequence; GMH, Gurla Mandhata–Humla fault system; Kcg, Kailas conglomerate; MBT, Main Boundary thrust; MCT, Main Central thrust zone; STD, South Tibetan Detachment; TSS, Tethyan Sedimentary Sequence.

plex by a bivergent detachment system – a structural system similar to that proposed for unroofing of the Menderes metamorphic core complex in western Turkey [*Gessner et al.*, 2001], and the Rhodope metamorphic core complex in northeast Greece [*Dinter*, 1998]. Horizontal shortening coeval with exhumation of rocks within the Gurla Mandhata metamorphic core complex is expressed by contractional fabrics concentrated within SZ 1 as well as large-scale east-west trending corrugations (Figures 3 and 4). We calculate 14% (6 km) of horizontal shortening in a direction N18°E (perpendicular to trend of corrugations).

[36] Contemporaneous with motion along the GMH is arc-normal contraction at more southward positions within the Himalayan fold-thrust belt. *DeCelles et al.* [1998] interpret the Dadeldhura thrust to initiate circa 15–14 Ma, the oldest age of the Siwalik Group. Sediment accumulation rates and magnetostratigraphic data from northern India suggest that the Main Boundary thrust (MBT) initiated circa 11 Ma [*Meigs et al.*, 1995], although *DeCelles et al.* [1998] interpret it to initiate at ~5 Ma in the Nepal Himalaya. Our results along the GMH indicate that the boundary between regions dominated by arc-parallel stretching and arc-normal contraction is located in the Lesser Himalaya between the MCT and MBT during the late Miocene.

5. Regional Structural Reconstruction

[37] In order to better understand the regional-scale geometry and evolution of the Karakoram fault system we

have constructed a map view restoration of the Karakoram fault (Figure 9). Our reconstruction is based on mapping by *Cheng and Xu* [1987], *Nakata* [1989], *Nakata et al.* [1990], *Yin et al.* [1999], *Searle et al.* [1998], *Murphy et al.* [2000], *Murphy et al.* [2002], *Kapp et al.* [2003], and this study.

[38] Figure 9a shows coeval development of the central strand of the Karakoram fault (35°N to 32°N), the GCT, and Shiquanhe thrust during the early to middle Miocene. The central strand of the Karakoram fault is a NNW striking right-slip shear zone and dips steeply to moderately toward the northeast [*Searle et al.*, 1998; *Murphy et al.*, 2000; *Kapp et al.*, 2003; *Lacassin et al.*, 2004] (Figure 9a). In the Zhaxigang area the shear zone displays ductile to brittle deformation from west to east. Results presented by *Searle* [1996] and *Searle et al.* [1998] indicate that the central strand of the Karakoram fault has accumulated a maximum of 150 km of right slip which is estimated from mapped offsets of Baltoro-type granites. Correlation of the Bangong-Nuijiang suture zone in Tibet with the Shyok suture zone in north Pakistan and Ladakh indicates ~120 km of right slip [*Searle et al.*, 1998; *Kapp et al.*, 2003] (Figure 9a). U-Pb ages of deformed and undeformed leucogranite dikes and sills in the Tangtse area indicate initiation of the Karakoram fault between 15.68 ± 0.52 and 13.73 ± 0.28 Ma [*Phillips et al.*, 2004] and a phase of rapid cooling of rocks bordering its western side beginning circa 11 Ma [*Dunlap et al.*, 1998]. South of Tangtse in the Zhaxigang area, U-Pb zircon ages of deformed and undeformed leucogranite dikes and sills indicate slip on the Karakoram fault initiated by 23 Ma. South of 32°N there is no evidence for movement on the Karakoram fault prior to 12 Ma [*Murphy et al.*, 2002; *Lacassin et al.*, 2004].

[39] Early movement (early to middle Miocene) on the central strand of the Karakoram fault is coeval with slip on the GCT (Figure 9a). The GCT is a regional north directed thrust system that has been mapped across the entire length of the Himalaya from northwest India to Eastern Tibet [*Heim and Gansser*, 1939; *Gansser*, 1964; *Ratschbacher et al.*, 1994; *Yin et al.*, 1999; *Murphy et al.*, 2000]. At all localities it is spatially associated with the suture between India and Asia (Indus-Yalu suture zone). The GCT juxtaposes Tethyan sedimentary rocks in its hanging wall against a >2.5-km-thick Oligocene–middle Miocene nonmarine clastic sedimentary sequence, referred to as the Kailas (or Gangrinboche) Conglomerate in Tibet and the Indus Molasse in India [*Gansser*, 1964; *Harrison et al.*, 1993; *Yin et al.*, 1999; *Aitchison et al.*, 2002]. Structural reconstructions across the GCT in the Mount Kailas area suggest the fault system has accommodated ~20 km of north-south shortening [*Murphy and Yin*, 2003]. The timing of slip on the GCT is constrained by the age of deposition and thermal history of the Kailas Conglomerate. The age of deposition has been estimated at three localities in western, central, and eastern Tibet [*Harrison et al.*, 1993; *Ryerson et al.*, 1995].

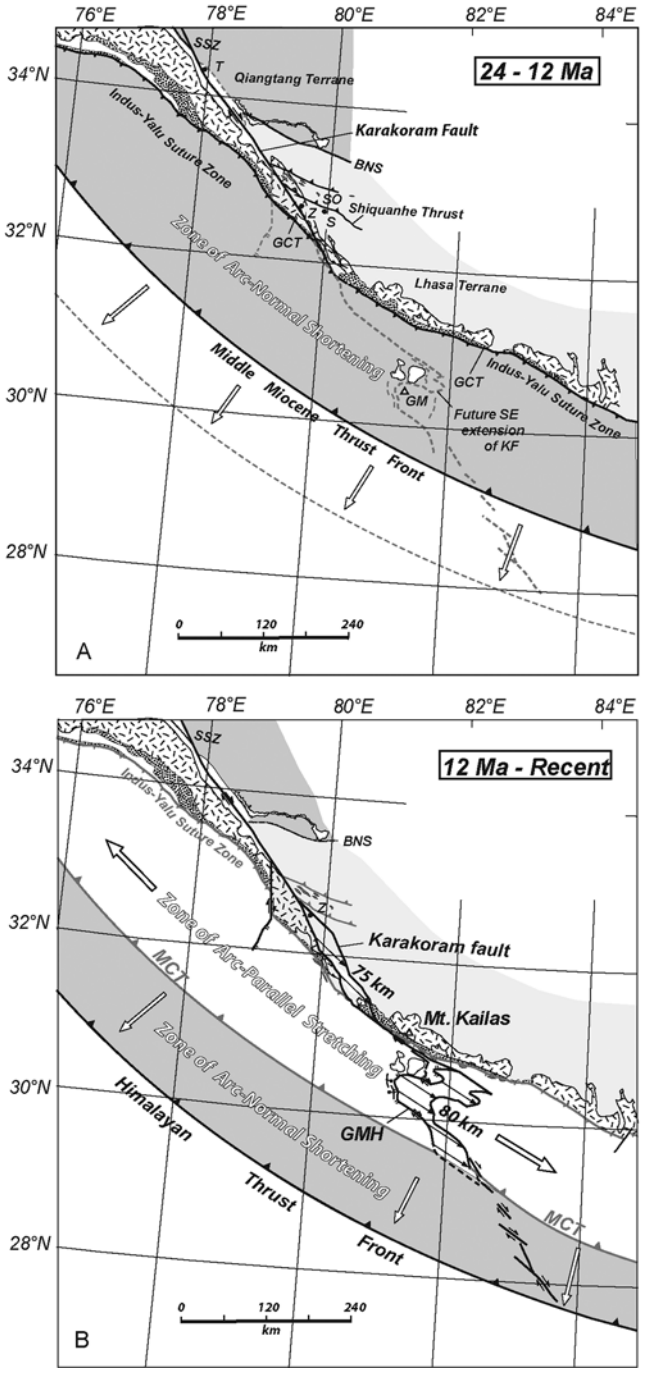

Figure 9. Map view reconstruction of the Karakoram fault since 24 Ma in a fixed India reference frame. See text for explanation. (a) Early to middle Miocene geologic setting of western Tibet and adjacent Himalayan fold-thrust belt. Karakoram fault is interpreted to either terminate or transfer slip into the GCT. (b) Foreland propagation of the Himalayan thrust front accompanied by lengthening of Karakoram fault into northwest Nepal. Karakoram fault feeds slip into the GMH, which cuts across the STD, MCT, and into the Lesser Himalaya. GMH extends east of our study area via active right-slip faults that feed into the MBT [*Nakata*, 1989; *Nakata et al.*, 1990]. Arrows and numbers along the Karakoram fault indicate the predicted magnitude and direction of slip on the Karakoram fault calculated from radial expansion model described in Figure 10.

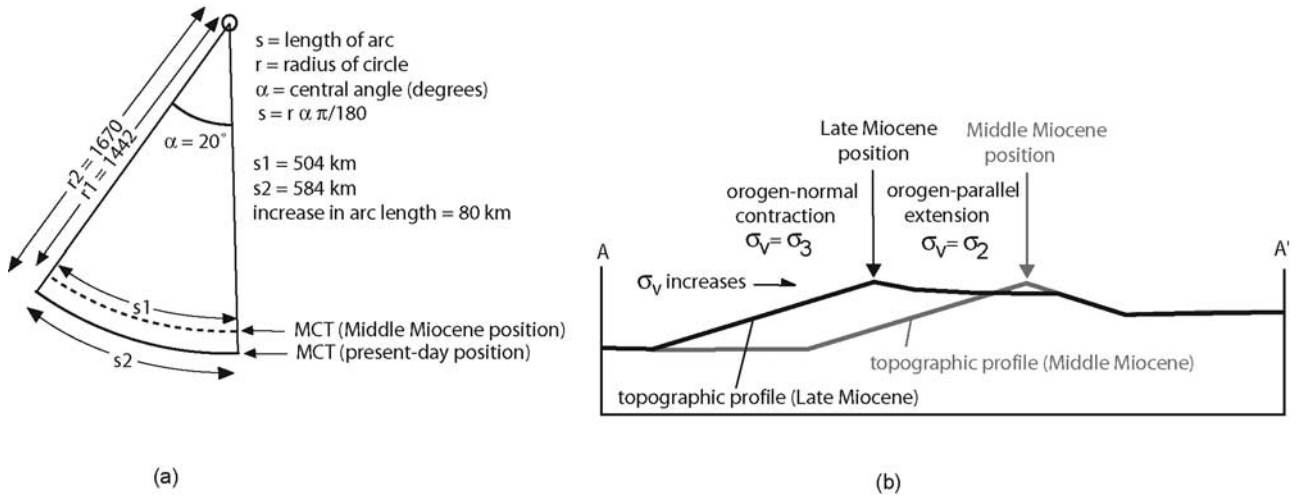

Figure 10. Schematic diagram showing possible evolution of the Himalayan topographic front in NW Nepal and SW Tibet. (a) Map view representation of the orogen described as a small circle centered at longitude 91.6° ± 1.6°E and latitude 42.4° ± 2.1° N [*Bendick and Bilham*, 2001]. Diagram illustrates the amount of orogen-parallel stretching resulting from 228 km of radial expansion along a 20° segment of the Himalayan orogen. (b) Representation of the topography across the Himalayan orogen during the middle Miocene and the late Miocene in a fixed India reference frame. The boundary between sections undergoing arc-normal contraction and arc-parallel extension is located at the back of the thrust wedge where we infer the vertical stress changes from the minimum principle stress to the intermediate or maximum principle stress. The topographic wedge propagates toward the foreland with the fold-thrust belt, thereby predicting that certain parts of the orogen pass from being located in regions undergoing arc-normal contraction to regions undergoing arc-parallel extension.

At all three sites, the results are consistent with a late Oligocene–early Miocene (30–17 Ma) age of deposition. On the basis of modeled K-feldspar $^{40}Ar/^{39}Ar$ data from clasts in the Kailas conglomerate in the footwall of the GCT, *Yin et al.* [1999] suggest that a temperature of 350°C was attained by 19 Ma and remained there until 13 Ma when a cooling rate of ~60°C/Myr began. The reheating event between 19 and 13 Ma is interpreted to reflect heating due to burial of the Kailas conglomerate by the hanging wall of the GCT. North of the GCT, field mapping in the Shiquanhe area shows that the Shiquanhe thrust is a south directed thrust fault that cuts 22.6 ± 0.3 Ma volcanic rocks and underlying deformed Tertiary strata [*Kapp et al.*, 2003] (Figure 9a). *Kapp et al.* [2003] estimate the Shiquanhe thrust to have accommodated 3–10 km of north-south shortening.

[40] Figure 9b shows 540 km lengthening of the Karakoram fault system from the Zhaxigang area to western Nepal. From Zhaxigang southward, the Karakoram fault strikes northwest cutting across the GCT (Indus-Yalu suture zone) and into the Tethyan fold-thrust belt [*Ratschbacher et al.*, 1994; *Murphy et al.*, 2000; *Murphy and Yin*, 2003; *Lacassin et al.*, 2004]. The geometry of the Karakoram fault in the Mount Kailas area and farther eastward is debated. *Lacassin et al.* [2004] suggest that the Karakoram fault extends eastward passed the Mount Kailas area following the Indus-Yalu suture zone (Figure 1). In contrast, *Murphy et al.* [2002] interpreted that the Karakoram fault linked with the Gurla Mandhata detachment system south of Mount Kailas (Figure 2). *Murphy et al.* [2002] speculated that the two faults linked in the vicinity of Mapam Yumco (large lake north of Gurla Mandhata (Figure 1). However, the presence of similar stratigraphic units on either side of the Mapam Yumco challenged the existence of a fault that accommodates a large amount of structural throw. Reconnaissance investigation of rocks due east of Mapam Yumco shows the presence of an east-west elongate gneiss dome (Figure 2). It is composed chiefly of garnet biotite quartzofeldspathic mylonitic gneisses. Stretching lineations dominantly plunge shallowly toward the west. Shear sense indicators show top-to-west sense of shear. Faults bordering the gneiss dome do not cut the Karakoram fault and therefore must be either younger or contemporaneous with motion along the Karakoram fault. Because the structural and lithologic characteristics of this gneiss dome are similar to that of the Gurla Mandhata metamorphic core complex we infer the timing of deformation also spanned the late Miocene. On the basis of these observations we suggest that ~65 km of slip on the Karakoram fault is transferred to the GMH at the intersection of the Karakoram fault and the northern boundary of the gneiss dome (82°E) (Figures 2 and 9a).

[41] Our proposed link requires the geometry of the fault system to change radically at the juncture of the Karakoram fault and the northern gneiss dome, from an east-west striking strike-slip fault to a north-south striking normal fault. This geometry is the same as that mapped in northwest Nepal (Figure 3). We speculate that the geometry of the Karakoram fault changes so radically because of the

highly heterogeneous nature of the crustal architecture. We envision that the generally northwest-southeast striking Karakoram fault extends across the Himalayan orogen by exploiting contacts between relatively "weak" and "strong" layers, such as that between the Indus-Yalu suture zone and the Indian passive margin sequence (TSS). In this scenario, the Karakoram fault steps southeastward to another "weak-strong" interface via north-south striking fault segments, a geometry similar to that recognized in thrust belts that display a ramp flat geometry.

[42] East of our study area in northwest Nepal we link the GMH to a system of northwest-southeast striking normal faults that extend across western Nepal [*Nakata*, 1989; *Nakata et al.*, 1990]. *Nakata et al.* [1990] noted that a Quaternary en echelon right-slip system extends across western Nepal cutting across the MCT zone and merges with the Main Boundary thrust in the central Nepal Himalaya (Figure 1). Moreover, GPS measurements from western Nepal delineate a crustal wedge within the Himalaya that is characterized by east-west (arc-parallel) extension [*Jouanne et al.*, 1999]. *Jouanne et al.* [1999] interpreted the southern margin of this wedge to lie along the southeast projection of the Karakoram fault system. Results from this study show that arc-parallel extension has been occurring within the High and Lesser Himalaya since the late Miocene.

6. Discussion

[43] Our reconstruction (Figures 9a and 9b) shows that the southeast tip of the Karakoram fault has merged with arc-normal contractional structures since the early Miocene. Below we suggest that the Karakoram fault acts as a transfer structure in a contractional setting that facilitates outward growth of the Himalayan orogen.

[44] Figures 10a and 10b show a conceptual model for outward expansion of the arcuate-shaped Himalayan fold-thrust belt. Approximately 228 km of shortening has been accounted for in the region between the Main Central thrust and the Main Frontal thrust in northwest India [*Srivastava and Mitra*, 1994] and in western Nepal [*DeCelles et al.*, 1998, and references therein]. Assuming a simple scenario whereby this amount of shortening is fed into a single top-south detachment implies that the hinterland region of the Main Central thrust has been translated toward the foreland for a distance of 228 km. Earthquake focal mechanisms and GPS-derived velocity fields indicate that the direction of overthrusting of the Himalaya onto the Indian shield is radially outward [*Baranowski et al.*, 1984; *Molnar and Lyon-Caen*, 1989; *Jade et al.*, 2004]. Figure 10a illustrates the amount of arc-parallel stretching resulting from radial expansion a 20° segment of the Himalayan orogen, roughly equivalent to the length of the southern portion of the Karakoram fault. The radius of curvature of the present-day position of the MCT is ~1670 km using the pole solution of *Bendick and Bilham* [2001]. The radius of curvature prior to shortening south of the MCT would have been 1442 km. Assuming the subducted plate (Indian Shield) behaves rigidly, requires ~80 km of arc parallel stretching to accommodate 228 km of radial expansion of the orogen (Figures 9b and 10a). Because individual thrusts in the fold-thrust belt get younger toward the thrust front, the age and magnitude of arc-parallel stretching also decreases toward the thrust front.

[45] We hypothesize that the Himalayan fold-thrust belt grows in this fashion through linked foreland propagating structural systems facilitating arc-normal contraction in the foreland and arc-parallel extension in the hinterland. We define the hinterland as the back of the thrust wedge at the interface between arc-normal contractional structures and arc-parallel extensional structures. We infer that this is the position where the vertical stress switches from being the minimum principle stress in the foreland to the intermediate or maximum principle stress in the hinterland. Figure 10b shows two hypothetical topographic profiles across the Himalayan orogen, one for the early to middle Miocene and another for the late Miocene. The topographic wedge propagates with the fold-thrust belt. The model predicts that parts of the orogen pass from being located in regions undergoing arc-normal contraction to regions undergoing arc-parallel extension. In this scenario, rocks in northwestern Nepal were in a region undergoing arc-normal contraction during the early to middle Miocene and later in a region undergoing arc-parallel extension during the late Miocene (Figure 10b).

[46] Any model to explain the tectonic evolution of the Himalaya since the late Miocene must incorporate a mechanism that accounts for transtensional deformation that shortly follows arc-normal shortening/thickening. Moreover, models that call upon late Miocene movement on the STD and within the MCT zone must explain the relationship between these faults with the GMH fault system. Below we evaluate previously proposed tectonic models that make predictions regarding the kinematics along the boundaries of the Tibetan Plateau (Figure 10). These models include (1) wholesale lateral extrusion [*Peltzer and Tapponnier*, 1988; *Armijo et al.*, 1989; *Pêcher*, 1991], (2) arc-parallel stretching [*Seeber and Armbruster*, 1984; *Molnar and Lyon-Caen*, 1989; *Coleman*, 1996; *Seeber and Pêcher*, 1998; *McCaffrey and Nabelek*, 1998], and (3) southward extrusion of Tibet by alternating periods of south directed thrusting and north directed normal faulting [*Hodges et al.*, 1996, 2001; *Beaumont et al.*, 2001]. The models listed above can be differentiated in terms of the kinematics that they prescribe along the southern margin of the Tibetan Plateau. The first two models emphasize orogen-parallel strike-slip faulting or extension along the southern margin of the Tibetan Plateau. Model 3 emphasizes north-south motion of the southern margin of the Tibetan Plateau.

[47] Model 3 considers the response of relatively weak crust to north-south crustal thickness gradient between the Tibetan Plateau and the Ganges plain. This model draws attention to the southward extrusion of Tibetan middle and lower crust as well as the GHC that is bounded above by the STD and below by the MCT zone [*Hodges et al.*, 1996; *Hodges*, 2000; *Beaumont et al.*, 2001]. Movement on the STD and MCT zone is interpreted to facilitate the southward extrusion of the middle crust. If model 3 is correct, our

work places some important limitations on the kinematics of the process: channelized flow after late Miocene time must not have been bound by the MCT and STD surfaces because the GMH transects both.

[48] The lateral extrusion model views the southern margin of the Tibetan Plateau as a zone of right-slip shear either located along the Indus-Yalu suture zone [*Peltzer and Tapponnier*, 1988] or along the South Tibetan Detachment System [*Pêcher*, 1991]. In each of these scenarios, the kinematics of the southern margin of the Tibetan Plateau, whether along the Indus-Yalu suture zone or the South Tibetan Detachment System, is thought to reflect eastward lateral extrusion of the Tibetan Plateau in response to India's northward indentation into Asia. The results from this study require significant modifications to the lateral extrusion hypothesis. First, the location of the southern boundary of the extruding block (Tibet) during the late Miocene would be along the GMH. This implies that the entire GHC, along with southern Tibet (Lhasa block), are apart of the same eastward extruding block. Second, *Peltzer and Tapponnier* [1988] and *Lacassin et al.* [2004] interpret 1000 and 600 km of right slip on the Karakoram fault system, respectively, resulting in significant eastward extrusion of Tibet. Subsequent studies along the Karakoram fault indicate that the total slip on the Karakoram fault is <150 km based on offset of the 20–17 Ma Baltoro–Tangtse granites [*Searle*, 1996; *Searle et al.*, 1998]. If our interpretation is correct that the Karakoram fault links to the GMH, our results limit the amount of possible eastward extrusion to a few tens of kilometers since the late Miocene. However, we cannot rule out the possibility that a portion of the slip on the Karakoram fault is transferred farther east as suggested by *Lacassin et al.* [2004].

[49] Models that appeal to arc-parallel stretching (strike-slip and normal faulting) emphasize the dynamics of deformation along the arcuate-shaped Himalayan front in controlling the kinematics along the western and southern margins of the Tibetan Plateau [*Seeber and Armbruster*, 1984; *Klootwijk et al.*, 1985; *Molnar and Lyon-Caen*, 1989; *Seeber and Pêcher*, 1998; *McCaffrey and Nabelek*, 1998]. In the context of these models, the GMH is a primary structure accommodating arc-parallel stretching. Between 180 and 100 km of arc-parallel stretching over the last 10 Myr is predicted by these models [*Molnar and Lyon-Caen*, 1989; *McCaffrey and Nabelek*, 1998]. Our slip estimates indicate that between 24% and 32% of elongation of the Himalayan orogen is accommodated along the GMH.

7. Conclusions

[50] 1. Geologic mapping in northwestern Nepal delineates a transtensional fault system referred to as the Gurla Mandhata–Humla fault system (GMH). The GMH cuts across the Tethyan fold-thrust belt, South Tibet Detachment, Greater Himalayan Crystalline sequence, the Main Central thrust zone, and into the Lesser Himalayan sequence.

[51] 2. $^{232}Th/^{208}Pb$ ion microprobe monazite ages from deformed and undeformed leucogranite bodies indicate the GMH was active between the middle to late Miocene. This timing estimate overlaps with those for the Dadeldhura and Main Boundary thrusts that are in more foreland positions within the Himalayan fold-thrust belt.

[52] 3. Contemporaneous arc-normal contraction and arc-parallel stretching is explained by a structural model calling upon linked foreland propagating structural systems facilitating arc-normal contraction in the foreland and arc-parallel extension in the hinterland. The boundary between these two structural domains is hypothesized to occur at the back of the thrust wedge where the vertical stress switches from being the minimum principle stress to the intermediate principle stress. Our kinematic model explains a mechanism that maintains the arcuate shape of the Himalayan orogen since the middle Miocene.

[53] **Acknowledgments.** This research was supported by National Science Foundation grant EAR- 0106808. Additional support was provided by the University of Houston GEAR program. We thank Paul Burgess for his assistance in the collection of structural data and Marty Grove for his assistance with the Th-Pb analyses. This manuscript was greatly improved by comments from Associate Editor Kip Hodges, Lothar Ratschbacher, An Yin, and an anonymous reviewer.

References

Aitchison, J. C., A. M. Davis, Badengzhu, and H. Luo (2002), New constraints on the India-Asia collision: The lower Miocene Gangrinboche conglomerates, Yarlung Tsangpo suture zone, SE Tibet, *J. Asian Earth Sci.*, *21*, 251–263.

Armijo, R., P. Tapponnier, and T. Han (1989), Late Cenozoic right-lateral strike-slip faulting in southern Tibet, *J. Geophys. Res.*, *94*, 2787–2838.

Avouac, J.-P., and P. Tapponnier (1993), Kinematic model of active deformation in central Asia, *Geophys. Res. Lett.*, *20*, 895–898.

Baranowski, J., J. G. Armbruster, L. Seeber, and P. Molnar (1984), Focal depths and fault-plane solutions of earthquakes and active tectonics of the Himalaya, *J. Geophys. Res.*, *89*, 6918–6928.

Beaumont, C., R. A. Jamieson, M. H. Nguyen, and B. Lee (2001), Himalayan tectonics explained by extrusion of a low-viscosity crustal channel coupled to focused surface denudation, *Nature*, *414*, 738–742.

Bendick, R., and R. Bilham (2001), How perfect is the Himalayan arc?, *Geology*, *29*, 791–794.

Brookfield, M. E. (1993), The Himalayan passive margin from Precambrian to Cretaceous, *Sediment. Geol.*, *84*, 1–35.

Burchfiel, B. C., Z. Chen, K. V. Hodges, Y. Liu, L. H. Royden, C. Deng, and J. Xu (1992), The South Tibetan Detachment System, Himalayan orogen: Extension contemporaneous with and parallel to shortening in a collisional mountain belt, *Spec. Pap. Geol. Soc. Am.*, *269*, 41 pp.

Burg, J.-P., and G. M. Chen (1984), Tectonics and structural formation of southern Tibet, China, *Nature*, *311*, 219–223.

Catlos, E. J., T. M. Harrison, M. J. Kohn, M. Grove, F. J. Ryerson, C. E. Manning, and B. N. Upreti (2001), Geochronologic and thermobarometric constraints on the evolution of the Main Central Thrust, central Nepal Himalaya, *J. Geophys. Res.*, *106*, 16,177–16,204.

Catlos, E. J., T. M. Harrison, C. E. Manning, M. Grove, S. M. Rai, M. S. Hubbard, and B. N. Upreti (2002), Records of the evolution of the Himalayan orogen from in situ Th-Pb ion microprobe dating of monazite: Eastern Nepal and western Garhwal, *J. Asian Earth Sci.*, *20*, 459–479.

Cheng, J., and G. Xu (1987), Geologic map of the Gerdake region at a scale of 1:1000000 and geologic report (in Chinese), 363 pp., Xizang Bur. of Geol. and Miner. Resour., Lhasa, China.

Coleman, M. E. (1996), Orogen-parallel and orogen-perpendicular extension in the central Nepalese Himalayas, *Geol. Soc. Am. Bull.*, *108*, 1594–1607.

Copeland, P., T. M. Harrison, and P. LeFort (1990), Age and cooling history of the Manaslu granite: Implications for Himalayan tectonics, *J. Volcanol. Geotherm. Res.*, *44*, 33–50.

DeCelles, P. G., G. E. Gehrels, J. Quade, T. P. Ojha, P. Kapp, and B. N. Upreti (1998), Neogene foreland

basin deposits, erosional unroofing, and kinematic history of the Himalayan fold-thrust belt, western Nepal, *Geol. Soc. Am. Bull.*, *110*, 2–21.

DeCelles, P. G., G. E. Gehrels, J. Quade, B. LaReau, and M. Spurlin (2000), Tectonic implications of U-Pb zircon ages of the Himalayan orogenic belt in Nepal, *Science*, *288*, 497–499.

DeCelles, P. G., D. M. Robinson, J. Quade, T. P. Ojha, C. N. Garzione, P. Copeland, and B. N. Upreti (2001), Stratigraphy, structure, and tectonic evolution of the Himalayan fold-thrust belt in western Nepal, *Tectonics*, *20*, 487–509.

Dinter, D. A. (1998), Late Cenozoic extension of the alpine collisional orogen, northeastern Greece: Origin of the north Aegean basin, *Geol. Soc. Am. Bull.*, *110*, 1208–1230.

Dunlap, W. J., R. F. Weinberg, and M. P. Searle (1998), Karakoram fault zone rocks cool in two phases, *J. Geol. Soc. London*, *155*, 903–912.

Edwards, M. A., and T. M. Harrison (1997), When did the roof collapse? Late Miocene north-south extension in the High Himalaya revealed by Th-Pb monazite dating of the Khulu Kangri granite, *Geology*, *25*, 543–546.

Gansser, A. (1964), *The Geology of the Himalayas*, 289 pp., Wiley Interscience, Hoboken, N. J.

Garzanti, E. (1999), Stratigraphy and sedimentary history of the Nepal passive margin, *J. Asian Earth Sci.*, *17*, 805–827.

Gessner, K., U. Ring, C. Johnson, R. Hetzel, C. W. Passchier, and T. Güngör (2001), An active bivergent rolling-hinge detachment system: Central Menderes metamorphic core complex in western Turkey, *Geology*, *29*, 611–614.

Godin, L., R. R. Parrish, R. L. Brown, and K. V. Hodges (2001), Crustal thickening leading to exhumation of the Himalayan Metamorphic core of central Nepal: Insight from U-Pb Geochronology and $^{40}Ar/^{39}Ar$ thermochronology, *Tectonics*, *20*, 729–747.

Harrison, T. M., P. Copeland, S. A. Hall, J. Quade, S. Burner, T. P. Ojha, and W. S. F. Kidd (1993), Isotopic preservation of Himalayan/Tibetan uplift, denudation, and climatic histories of two molasses deposits, *J. Geol.*, *100*, 157–175.

Harrison, T. M., K. D. McKeegan, and P. LeFort (1995), Detection of inherited monazite in the Manaslu leucogranite by $^{208}Pb/^{232}Th$ ion microprobe dating: Crystallization age and tectonic implications, *Earth Planet. Sci. Lett.*, *133*, 271–282.

Harrison, T. M., F. J. Ryerson, P. Le Fort, A. Yin, O. M. Lovera, and E. J. Catlos (1997), A late Miocene-Pliocene origin of for the central Himalayan inverted metamorphism, *Earth Planet. Sci. Lett.*, *146*, E1–E8.

Harrison, T. M., M. Grove, O. M. Lovera, and E. J. Catlos (1998), A model for the origin of Himalayan anatexis and inverted metamorphism, *J. Geophys. Res.*, *103*, 27,017–27,032.

Hauck, M. L., K. D. Nelson, L. D. Brown, W. Zhao, and A. R. Ross (1998), Crustal structure of the Himalayan Orogen at ~90° east longitude from Project INDEPTH deep reflection profiles, *Tectonics*, *17*, 481–500.

Heim, A., and A. Gansser (1939), Central Himalaya, geological observations of the Swiss expeditions 1936, *Mem. Soc. Helv. Sci. Nat.*, *LXXII*, 245 pp.

Hodges, K. V. (2000), Tectonics of the Himalaya and southern Tibet from two perspectives, *Geol. Soc. Am. Bull.*, *112*, 324–350.

Hodges, K. V., R. R. Parrish, T. B. Housh, D. R. Lux, B. C. Burchfiel, L. H. Royden, and Z. Chen (1992), Simultaneous Miocene extension and shortening in the Himalayan orogen, *Science*, *258*, 1466–1470.

Hodges, K. V., R. R. Parrish, and M. P. Searle (1996), Tectonic evolution of the central Annapurna range, Nepalese Himalaya, *Tectonics*, *15*, 1264–1291.

Hodges, K. V., S. Bowring, K. Davidek, D. Hawkins, and M. Krol (1998), Evidence for rapid displacement on Himalayan normal faults and the importance of tectonic denudation in the evolution of mountain ranges, *Geology*, *26*, 483–486.

Hodges, K. V., J. M. Hurtado, and K. X. Whipple (2001), Southward extrusion of Tibetan crust and its effect on Himalayan tectonics, *Tectonics*, *20*, 799–809.

Hubbard, M., and T. M. Harrison (1989), $^{40}Ar/^{39}Ar$ age constraints on deformation and metamorphism in the Main Central Thrust zone and Tibetan Slab, eastern Nepal Himalaya, *Tectonics*, *8*, 865–880.

Hurtado, J. M., K. V. Hodges, and K. X. Whipple (2001), Neotectonics of the Thakkhola graben and implications for recent activity on the South Tibetan fault system in the central Nepal Himalaya, *Geol. Soc. Am. Bull.*, *113*, 222–240.

Jade, S., B. C. Bhatt, Z. Yang, R. Bendick, V. K. Gaur, P. Molnar, M. B. Anand, and D. Kumar (2004), GPS measurements from the Ladakh Himalaya, India: Preliminary tests of plate-like or continuous deformation in Tibet, *Geol. Soc. Am. Bull.*, *116*, 1385–1391.

Jouanne, F., J. L. Mugnier, M. R. Pandey, J. F. Gamond, P. LeFort, L. Serrurier, C. Vigny, and J. P. Avouac (1999), Oblique convergence in the Himalayas of western Nepal deduced from preliminary results of GPS measurements, *Geophys. Res. Lett.*, *26*, 1933–1936.

Kapp, P., M. A. Murphy, A. Yin, T. M. Harrison, L. Ding, and J. Guo (2003), Mesozoic and Cenozoic tectonic evolution of the Shiquanhe area of western Tibet, *Tectonics*, *22*(4), 1029, doi:10.1029/2001TC001332.

Klootwijk, C. T., P. J. Conaghan, and C. M. Powell (1985), The Himalayan Arc: Large-scale continental subduction, oroclinal bending and back-arc spreading, *Earth Planet. Sci. Lett.*, *75*, 167–183.

Lacassin, R., et al. (2004), Large-scale geometry and offset of the Karakoram fault, Tibet, *Earth Planet. Sci. Lett.*, *219*, 255–269.

Lee, J., B. R. Hacker, W. S. Dinklage, Y. Wang, P. Gans, A. Calvert, J. Wan, W. Chen, A. E. Blythe, and W. McClelland (2000), Evolution of the Kangmar Dome, southern Tibet: Structural, petrologic, and thermochronologic constraints, *Tectonics*, *19*, 872–895.

Macfarlane, A. M. (1993), Chronology of tectonic events in the crystalline core of the Himalaya, Langtang National Park, central Nepal Himalaya, *Tectonics*, *12*, 1004–1025.

Makovsky, Y., S. L. Klemperer, L. Ratschbacher, and D. Alsdorf (1999), Midcrustal reflector on INDEPTH wide-angle profiles: An ophiolitic slab beneath the India-Asia suture in southern Tibet, *Tectonics*, *18*, 793–808.

McCaffrey, R., and J. Nabelek (1998), Role of oblique convergence in the active deformation of the Himalayas and southern Tibet plateau, *Geology*, *26*, 691–694.

Meigs, A. J., D. W. Burbank, and R. A. Beck (1995), Middle-late Miocene (>10 Ma) formation of the Main Boundary Thrust in the western Himalaya, *Geology*, *23*, 423–426.

Molnar, P., and H. Lyon-Caen (1989), Fault plane solutions of earthquakes and active tectonics of the Tibetan Plateau and its margins, *Geophys. J. Int.*, *99*, 123–153.

Murphy, M. A. (2000), Tectonic evolution of western Tibet, Ph.D. dissertation, 221 pp., Univ. of Calif., Los Angeles.

Murphy, M. A., and T. M. Harrison (1999), Relationship between leucogranites and the Qomolangma detachment in the Rongbuk Valley, south Tibet, *Geology*, *27*, 831–834.

Murphy, M. A., and A. Yin (2003), Structural evolution and sequence of thrusting in the Tethyan fold-thrust belt, *Geol. Soc. Am. Bull.*, *115*, 21–34.

Murphy, M. A., A. Yin, P. Kapp, T. M. Harrison, L. Ding, and J. Guo (2000), Southward propagation of the Karakoram fault system, southwest Tibet: Timing and magnitude of slip, *Geology*, *28*, 451–454.

Murphy, M. A., A. Yin, P. Kapp, T. M. Harrison, and C. E. Manning (2002), Structural and thermal evolution of the Gurla Mandhata metamorphic core complex, southwest Tibet, *Geol. Soc. Am. Bull.*, *114*, 428–447.

Nakata, T. (1989), Active faults of the Himalaya of India and Nepal, in *Tectonics of the Western Himalaya*, edited by L. L. Malinconico and R. J. Lillie, *Spec. Pap. Geol. Soc. Am.*, *232*, 243–264.

Nakata, T., K. Otsuki, and S. H. Khan (1990), Active faults, stress field, and plate motion along the Indo-Eurasian plate boundary, *Tectonophysics*, *181*, 83–95.

Parrish, R. R. (1990), U-Pb dating of monazite and its application to geological problems, *Can. J. Earth Sci.*, *27*, 1431–1450.

Parrish, R. R., and K. V. Hodges (1996), Isotopic constraints on the age and provenance of the Lesser and Greater Himalayan sequences, Nepalese Himalaya, *Geol. Soc. Am. Bull.*, *108*, 904–911.

Pearson, O. N. (2002), Structural evolution of the central Nepal fold-thrust belt and regional tectonic and structural significance of the Ramgarh thrust, Ph.D. dissertation, 231 pp., Univ. of Ariz., Tucson.

Pêcher, A. (1991), The contact between the Higher Himalaya crystallines and the Tibetan sedimentary series: Miocene large-scale dextral shearing, *Tectonics*, *10*, 587–598.

Peltzer, G., and P. Tapponnier (1988), Formation and evolution of strike-slip faults, rifts, and basins during the India-Asia collision: An experimental approach, *J. Geophys. Res.*, *93*, 15,085–15,117.

Phillips, R., R. R. Parrish, and M. P. Searle (2004), Age constraints on ductile deformation and long-term slip rates along the Karakora fault zone, Ladakh, *Earth Planet. Sci. Lett.*, *226*, 305–319.

Ratschbacher, L., W. Frisch, and G. Liu (1994), Distributed deformation in southern and western Tibet during and after the India-Asia collision, *J. Geophys. Res.*, *99*, 19,917–19,945.

Replumaz, A., and P. Tapponnier (2003), Reconstruction of the deformed collision zone Between India and Asia by backward motion of lithospheric blocks, *J. Geophys. Res.*, *108*(B6), 2285, doi:10.1029/2001JB000661.

Robinson, D. M. (2001), Structural and Nd-isotopic evidence for the tectonic evolution of the Himalayan fold-thrust belt, western Nepal and the northern Tibetan Plateau, unpublished Ph.D. dissertation, 224 pp., Univ. of Ariz., Tucson.

Robinson, D. M., P. G. DeCelles, C. N. Garzione, O. N. Pearson, T. M. Harrison, and E. J. Catlos (2003), Kinematic model for the Main Central Thrust in Nepal, *Geology*, *31*, 359–362.

Rothery, D. A., and S. A. Drury (1984), The neotectonics of the Tibetan Plateau, *Tectonics*, *3*, 19–26.

Ryerson, F. J., T. M. Harrison, A. Yin, and M. A. Murphy (1995), The Gangdese and Renbu-Zedong thrust systems: Westward extension to Mt. Kailas, *Geol. Soc. Am. Abstr. Programs*, *27*, 335.

Searle, M. P. (1986), Structural evolution and sequence of thrusting in the High Himalayan, Tibetan-Tethys and Indus suture zones of Zanskar and Ladakh, western Himalaya, *J. Struct. Geol.*, *8*, 923–936.

Searle, M. P. (1996), Geological evidence against large-scale pre-Holocene offsets along the Karakoram fault: Implications for the limited extrusion of the Tibetan Plateau, *Tectonics*, *15*, 171–186.

Searle, M. P., R. R. Parrish, K. V. Hodges, A. Hurford, M. W. Ayres, and M. J. Whitehouse (1997), Shisha Pangma leucogranite, south Tibetan Himalaya: Field relations, geochemistry, age, origin, and emplacement, *J. Geol.*, *105*, 295–317.

Searle, M. P., R. F. Weinberg, and W. J. Dunlap (1998), Transpressional tectonics along the Karakoram fault zone, northern Ladakh: Constraints on Tibetan extrusion, in *Continental Transpressional and Transtensional Tectonics*, edited by R. E. Holdsworth et al., *Geol. Soc. Spec. Publ.*, *135*, 307–326.

Seeber, L., and J. G. Armbruster (1984), Some elements of continental subduction along the Himalayan front, *Tectonophysics*, *105*, 263–278.

Seeber, L., and A. Pêcher (1998), Strain partitioning along the Himalayan arc and the Nanga Parbat antiform, *Geology*, *26*, 791–794.

Shrestha, S. B., S. R. Shrestha, and S. R. Sharma (Compilers) (1987), Geologic map of far western Nepal, 1:250,000 scale, Dep. of Mines and Geol., Kathmandu.

Srivastava, P., and G. Mitra (1994), Thrust geometries and deep structure of the outer and lesser Himalaya, Kumaon and Garhwal (India): Implications for evolution of the Himalayan fold-and-thrust belt, *Tectonics*, *13*, 89–109.

Tapponnier, P., G. Peltzer, A. Y. Le Dain, and R. Armijo (1982), Propagating extrusion tectonics in Asia: New insights from simple experiments with plasticine, *Geology*, *10*, 611–616.

Taylor, M., A. Yin, F. J. Ryerson, P. Kapp, and L. Ding (2003), Conjugate strike-slip faulting along the Bangong-Nujiang suture zone accommodates coeval east-west extension and north-south shortening in the interior of the Tibetan Plateau, *Tectonics*, *22*(4), 1044, doi:10.1029/2002TC001361.

Tullis, J., and R. A. Yund (1991), Diffusion creep in feldspar aggregates: Experimental evidence, *J. Struct. Geol.*, *13*, 987–1000.

Upreti, B. N. (1999), An overview of the stratigraphy and tectonics of the Nepal Himalaya, *J. Asian Earth Sci.*, *17*, 577–606.

Valdiya, K. S. (1981), Tectonics of the central sector of the Himalaya, in *Zagros-Hindu Kush-Himalaya: Geodynamic Evolution*, *Geodyn. Ser.*, vol. 3, edited by H. K. Gupta and F. M. Delany, 87–111, AGU, Washington, D. C.

Valdiya, K. S. (1989), Trans-Himadri intracrustal fault and basement upwarps, in *Tectonics of the Western Himalaya*, edited by L. L. Malinconico and R. J. Lillie, *Spec. Pap. Geol. Soc. Am.*, *232*, 153–168.

Wright, T. J., B. Parsons, P. C. England, and E. J. Fielding (2004), InSAR observations of low slip rates on major faults in western Tibet, *Science*, *305*, 236–239.

Yin, A. (2005), Cenozoic evolution of the Himalayan orogen as constrained by along-strike variations of structural geometry, exhumation history, and foreland sedimentation, *Earth Sci. Rev.*, in press.

Yin, A., and T. M. Harrison (2000), Geologic evolution of the Himalayan-Tibetan orogen, *Annu. Rev. Earth Planet. Sci.*, *28*, 211–280.

Yin, A., T. M. Harrison, M. A. Murphy, M. Grove, S. Nie, F. J. Ryerson, X. Wang, and Z. Chen (1999), Tertiary deformation history in southeastern and southwestern Tibet during the Indo-Asian collision, *Geol. Soc. Am. Bull.*, *111*, 1644–1664.

Yin, J., J. Xu, C. Liu, and H. Li (1988), The Tibetan Plateau: Regional stratigraphic context and previous work, *Philos. Trans. R. Soc. London, Ser. A*, *327*, 5–52.

P. Copeland and M. A. Murphy, Department of Geosciences, University of Houston, Houston, TX 77204-5007, USA. (mmurphy@mail.uh.edu)